Instituto Tecnológico y de Estudios Superiores de Monterrey

Campus Monterrey

School of Engineering and Sciences

Design Methodology of an Energy Harvesting damper for Automotive Suspension

A dissertation presented by

Kevin Alejandro Garcia Escalante

Submitted to the

School of Engineering and Sciences

in partial fulfillment of the requirements for the degree of

Master of Science

In

Manufacturing Systems

Monterrey, Nuevo Leon, June 10th, 2022

Dedication

I dedicate my dissertation work to my family. A special feeling of gratitude to my loving parents, Marcelo and Rosario whose words of encouragement and push for tenacity have motivated me during all this work. My brothers Marcelo, and Andrés have never left my side, helped me in difficult times, and they have made this journey an incredible experience. I am truly thankful for having you all in my life. Finally, I would like to dedicate this work to my past self,you can achieve everything you set your mind.

.

Acknowledgements

I would like to express my gratitude to all those who have supported me throughout this journey. I would like to first start by thanking my advisor, Dr. Jorge de Jesús Lozoya, for guidance during this work as well as give me the opportunity to work with him.

I would also like to thank my Co-Advisor, Dr. Renato Galuzzi, for being always a source of guidance, letting me join his on going project related to Regenerative dampers and provide me with all the knowledge needed to develop this work.

I would like to thank all of the committee members, Dr. Juan Carlos Tudón, and Msc. Salvatore Circosta, for their invaluable feedback and recommendations.

I thank CONACYT and Instituto Tecnológico y de Estudios Superiores de Monterrey for its financial support and for hosting me during these years.

Finally, I am grateful to my family and new friends that made these years of research an agreeable and pleasant journey.

Design Methodology of an Energy Harvesting damper for Automotive Suspension

by

Kevin Alejandro Garcia Escalante

Abstract

Energy loses in automobile cars now a days are very important, because of climate change everything is turning in to circular economy, green energy and to regenerate as much energy as possible. To improve fuel economy in cars, reducing Co2 emissions and supply other power demand systems, recovery systems were developed such as the regenerative braking energy and others are gaining attention like the vibration energy recovery on shock absorbers.

Therefore, this energy dissipated through the shock absorber as heat can be transformed into electricity and stored in a battery for other use in the vehicle. The presented work provides a solution to regenerate energy through a transmission coupled with an Electric Motor. The main contribution of this research project is the implementation of a Cycloid Drive which was never used for this type of application and its totally new in the state of the art.

The second main contribution is the optimization design methodology to couple both components together, the Electric Motor model and the Cycloid Drive model. A way to link them is presented, and several tests are performed with the parameters of the EV-TEC.

List of Figures

List of Tables

Contents

Table of Contents

1 Introduction

1.1 Motivation

Reducing vehicle energy losses now a days is very important to improve fuel economy, reducing CO_2 [1] emissions and supply other power demand systems. To achieve this, many recovery systems were developed such as the regenerative braking energy and others are gaining attention like the vibration energy recovery on shock absorbers [2].

Vehicles are submitted to different kind of road profiles which cause the suspension to move. This energy is dissipated through the shock absorber as heat [3]. The energy dissipated can be transformed into electricity and stored in a battery for other use in the vehicle [4].

Among many harvesting systems, the most popular are the electromagnetic motors because of the high energy conversion efficiency, fast response, controllability, and energy recovery capability [3].

According to Zuo and Zhang [4] the energy that can be obtained from a city small car is around 100 and 40 W at 97 km/h obtaining a 300W of electrical power and a 3% of improvement in fuel efficiency. Levant engineers based on their tests reported in average 1000 W in a truck on highway [5]. Audi reported a 3g/km of possible reduction of carbon dioxide for hybrid cars in a small car also an improvement of fuel economy by 0.7L /100 km [6].

The amount of energy that can be harvested has a relation with the intensity of oscillations of the suspension, which means that the more aggressive, the more energy can be harvested [4].

The mechanisms required for the energy harvesting have been investigated to increase fuel efficiency to then use them to recharge the car batteries, supply energy to the A/C or to power an active or semi active suspension to enhance comfort, ride quality and road handling [4].

The purpose of this work is adding an innovative gearbox that will receive a great torque as input and a high speed out put that will go to the electric motor that will supply a battery with electricity that later could be used for other car applications.

1.2 Problem Statement

The amount of energy that can be collected is related to the intensity of oscillations which means, more aggressive is equal to more energy harvested [7]. Oscillations depend on the conditions of the road, but the energy harvested also depend in the efficiency of the elements in charge for the harvesting. According to Abdelkareem, simple to construct rotary motion transmissions have greater efficiency. Among the transmissions presented in his work, the rack pinion is the most effective, but the problem lies with the conversion efficiency which is around 5 to 70% of the regenerated power of 250 W, which can be enhanced with a different mechanical transmission and other problem is the size it occupies in the suspension which complicates its implementation in other cars [4].

The objective of this work is to solve these two main problems by implementing a mechanical transmission with less size and high-speed output which therefore will substitute the regular shock absorber with a regenerative shock absorber.

1.3 Research questions

The implementation of a Cycloidal Drive could be a compact component in the suspension, and it can also replace the regular hydraulic shock absorbers on the rear axles.

This work intends to prove the feasibility of a Cycloid Drive and the possibility of substituting the standard shock absorbers in the vehicle.

1. Is a Cycloid regenerative shock absorber suitable for replacing a regular shock absorber?
2. Can a cycloid regenerative shock absorber design satisfy the required constraints for a vehicle damping task?

1.4 Solution overview

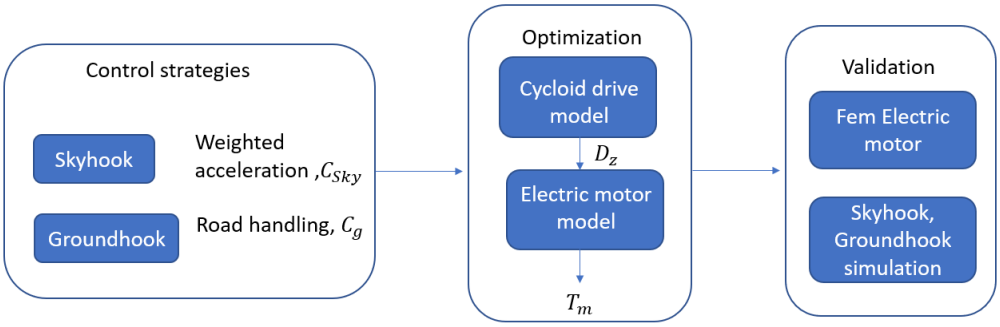

Fig. 1 **Solution Overview.**

To solve this problematic according to the state of the art, the rotary motion transmissions are better in terms of efficiency and regenerated energy [5]. The gearbox that is proposed in this work is a Cycloid Drive that has a high torque input attached to the control arm of the suspension and substituting the standard hydraulic shock absorber. The high rpm output is connected to an electric motor that will supply electricity to a battery that can contribute with the demand of energy of the accessories of the vehicle or to control an active or semiactive suspension.

First, two control strategies are presented with the parameters of an electric vehicle called EV-TEC. From this control strategies two values are obtained, the weighted acceleration and C_{Sky} for the Skyhook and the Road handling, C_g for the Groundhook. Second, the optimization is performed with particle swarm for the Cycloid Drive with 5 design variables and 1 objective function. Then, the D_z design variable of the Cycloid drive model is the input of the Electric Motor model to then obtain the T_m torque of the motor. Next, for the validation of the electric torque motor a FEM numerical analysis of the electric motor is performed and finally, the validation is performed in Simscape of both control strategies with the Cycloid regenerative shock absorber, which is the Cycloid drive and

electric motor together and compare the values of weighted acceleration and Road handling with the values obtained in the first step.

1.5 Main Contributions

The implementation of a Cycloid Drive as a rotary gearbox is completely new to the area, there is no reference in the state of the art of a cycloid mechanism to be part of an electromagnetic mechanism and to work as a shock absorber completely substituting regular hydraulic dampers.

Another important contribution is the implementations of new optimization strategies that are not used in this field such as Particle Swarm algorithm.

1.6 Dissertation organization

In Chapter 1, the problematic is defined, followed by possible solutions, also a brief background of types of vehicle-suspension systems are introduced. A literature review of related research results on vehicle suspension systems is also discussed. Specifically, in this chapter various types of regenerative suspensions are considered and compared.

In Chapter 2, the reference car suspension system is represented in a quarter-car model. and performance indexes are obtained. An overview of the different Iso Road profiles is presented, and the capabilities of the regenerative suspension system are investigated. Finally, different active strategies are presented, such as the Skyhook and Ground hook.

In Chapter 3, the gearbox selection is discussed. Then, a gearbox model is proposed as well as an electric motor. Next, the optimization strategy and output are analyzed.

In Chapter 4, the validation for the values obtained in the Skyhook and Groundhook configurations with the regenerative shock absorber are compared to the values obtained in chapter 2. Cycloid shock absorber is presented with the final values of the optimization and CAD representations and positioning in the vehicle chassis EV-TEC.

In Chapter 5, the conclusions of this research are stated, and future work is discussed.

1.7 Background (antecedents)

In this section, vehicle suspensions are explained and the different suspension systems such as passive suspension system, semi active suspension, and active suspension with their corresponding example in the car industry. At the end a comparative table with all the technologies working as damper or actuator for better understanding the differences.

1.7.1 Vehicle suspension system

One of the main systems of the vehicle is the suspension which main task is to minimize the vibrations transmitted from the terrain, and at the same time have comfort while riding. A regular suspension mainly consists of a sprung mass which is the body of the car, the unsprang masses which are the car wheels, the springs and dampers in every corner. As the vehicle moves over the road profile, the disturbance of the type of road acts as input of displacement [8]. Meanwhile, springs and dampers filter the vibrations stopping vibration transfer to the sprung mass [8]. The suspension systems in general are classified as regular passive, semi active which are the most common, and active suspension systems that are mainly for comfort. Passive suspension systems are the most common due to its market value which is not expensive. In this type of suspensions, a constant value is set up fix. Following the list semi active systems modify the damping coefficient according to the road input to provide better comfort. The innovative systems is the active suspension systems that consist of an actuator to minimize the road profile excitation and as a consequence achieve impressive comfort [9].

1.7.1.1 Passive suspension system

The passive suspensions are the most common commercially. Designed to minimize the excitation energy by using fluid and cavities in the damper, they are affordable and stand out for simple design. The passive system consists of a spring and a damper that depending on the type of suspension varies [8]. A softer damper can provide better comfort, in the other hand a damper with stiff characteristic is mainly for stable riding. The passive suspension system is set up to a point where can respond to most of the road classes. The draw back about them is that if the road conditions vary constantly is complicated to change all dampers every time.

The shock absorber a piston is positioned [9], with oil inside, which reacts to the demand of the terrain perturbances. The oil goes into cavities passing valves. A rod inside the damper varies in volume while the process takes place.

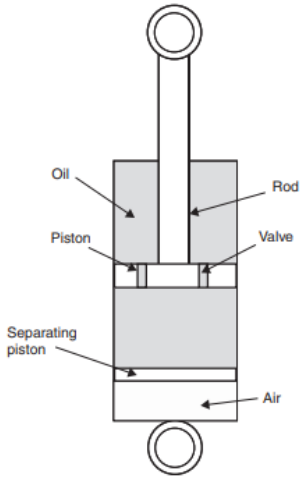

Fig. 2 **Passive damper** [9]**.**

$Fshock$ consists of three forces presented as:

$$F_{Shock} = F_d\,(\mathrm{x}, \dot{x}) + F_{air}(\mathrm{x}) + F_0 \mathrm{sign}(\dot{x}) \quad (1)$$

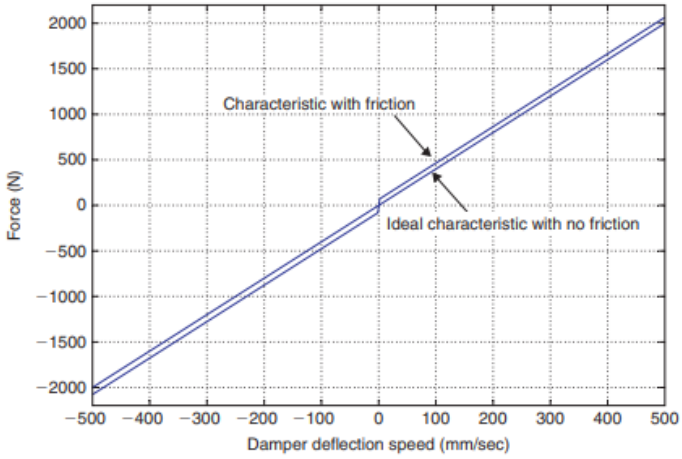

Fig. 3 **Passive damper behavior.** [9]

The damping force is presents as F_d. The force response by the air is F_{air}, and the friction force is F_0.

Fig. 4 **Passive damper BWI group.** [11]

1.7.1.2 Semi-active suspension system

Semi-active suspensions use external power to vary the damping force when the automobile experience different irregular road profile inputs. When a bump is hit by the automobile, the controller and the sensor take the signal input and vary the damper to mitigate the vibration in a short time [9]. Damping variation of is achieved by the technologies presented:

- Electrohydraulic Dampers

  The working principals are similar to the passive damper ,but with the difference that it has a electric valve that varies according to the signal it receives.

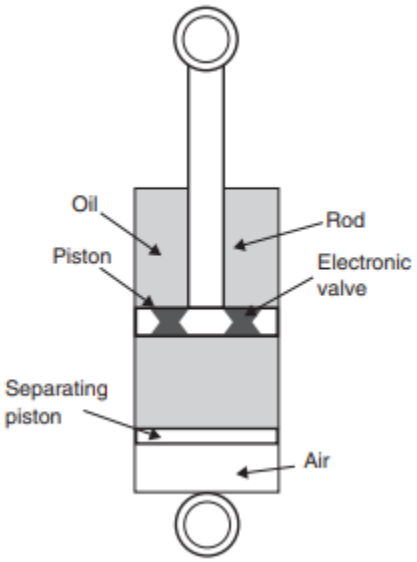

Fig. 5 **Electrohydraulic shock absorber.** [9]

Fig 5. corresponds to a real semiactive catalog from Bilstein [13].It is just for illustrative purpose, it has no scale, it basically shows that in the first and third quadrant there is a damping response,

but because automotive companies like to show a negative damping force with positive velocity it is shown as in fig 6.

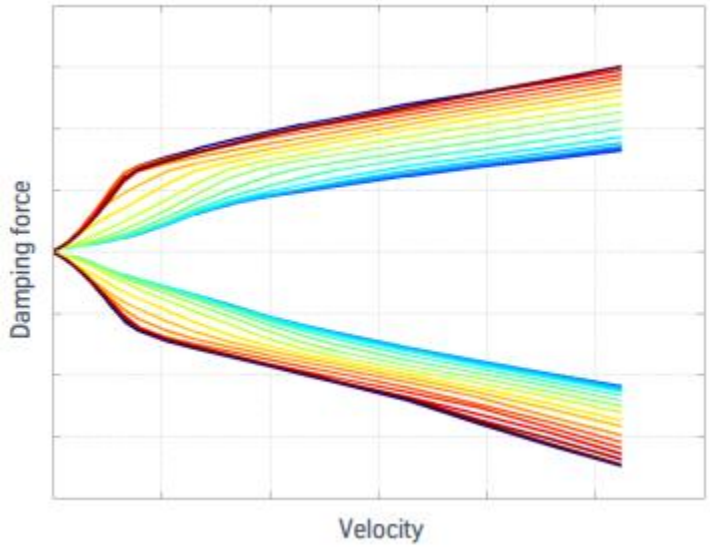

Fig. 6 **Damping vs velocity.** [13]

- Magnetorheological Dampers

  Magnetorheological dampers working principle consists of modifying the viscosity by applying a magnetic field. It is formed with oil and sensitive particles that are microscopic that react to the magnetic field. The behavior of a liquid when a field is not applied varies. When the fluid is submitted to a magnetic field, the microscopic particles cause react chains and the result is a viscous fluid [9].

A semi active suspension system is a more advance that a traditional passive suspension because a quicker response in real time is achieved. But a drawback is that when the system breaks, the suspension system works as a regular damper. The MR-fluid damper is one of the most common types of semiactive suspension that can be set up depending on the road conditions the car commonly faces. However, the problem is with the cost of MR-fluid dampers which are expensive, and is important to mention that with time MR properties with time are affected negatively, sealing problems, heat is common.

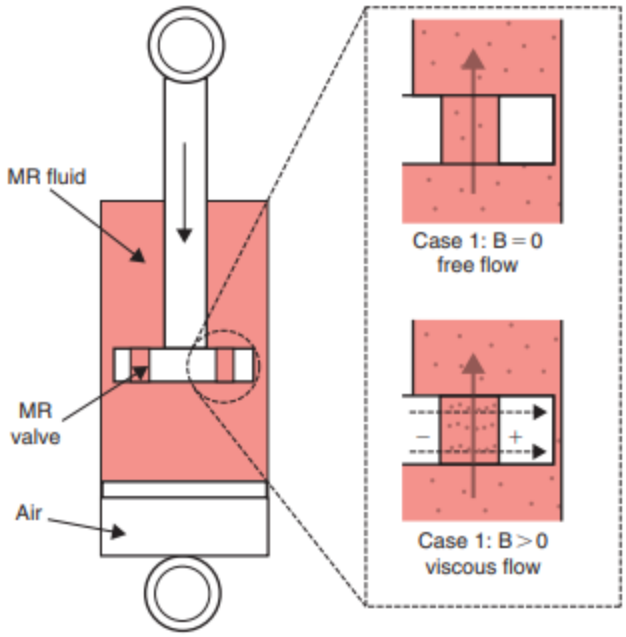

Fig. 7 **Magnetorheological damper behavior.** [9]

Fig. 8 **Semi active suspension Volvo XC90.** [14]

- Electrorheological Dampers

  With a similar behavior to a damper that is magnetorheological , electrorheological dampers function by varying the damping with the fluid flow properties inside the shock absorber. A mix

of micron and oil sized particles which are sensible to electric fields. If the electric field is not applied, the fluid flows free in the cavities of the damper, but when the electric field occurs, particles create chains, so that a visco plastic is formed from an almost free fluid [9].

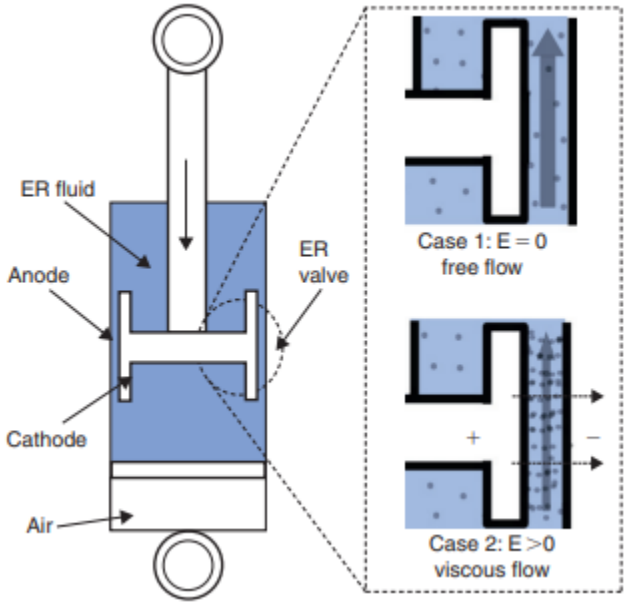

Fig. 9 **Electrorheological damper with and without electric field.** [9]

1.7.1.4 Active suspension system

An active suspension system use power from the vehicle to minimize the vibrations in the car compartment. The active suspension system performance work with different type of control strategies to enhance comfort. The way it works is with an actuator that applies an external force to diminish the sprung mass vibrations [15]. However, active suspensions are mainly in high end vehicles with suspensions that have enough space for placing the actuator mechanism without interfering vehicle dynamics and that are capable of supplying enough energy for the actuator to work. But if there is cut in energy supply to the actuator, the vehicle has no reaction to the road profile and no damping creating a complex and compromise scenario being safety a main concern for active suspension systems.

Fig. 10 **Active Body Control** [13].

The energy needed for the suspension to work is supplied by the engine of the car, through a hydraulic pump that is controlled by a unit control to decide the behavior of the suspension. It is important to mention that this active body control demands a lot of energy in other to Increase comfort without regenerating energy [13].

Table 1 **Controllable suspensions** [9].

System class	Control range (spring)	Control range (damper)	Control bandwidth	Power request	Control variable
Passive	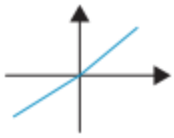	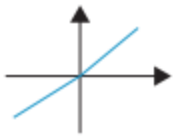	-	-	-
Semi-active	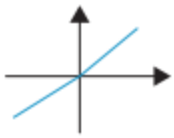		30–40 Hz	10–20 W	*c (damping ratio)*
Fully active			20–30 Hz	5–10 kW	*F (force)*

In Table 1 three features are very important to highlight the control bandwidth, the power request and the control variable [9].\

Three system class are presented in table 1, passive semi active and fully active.

Semi-active suspension systems work by modifying the damping coefficient in the quadrants one an three around a bandwidth of 30 to 40 Hz [9]. The forces that are deliverable have the constraint of a passivity damper. Thus, into the system there is no energy introduced. Thus, because of these features, the power requested is minimal.

Fully active suspensions work with an actuator that has the faster time in response with a bandwidth of 20 to 30 Hz [9]. Force F is the control variable in most of the control strategies in the market. The bandwidth that is available is the same as suspensions that are semi-active. However, because the range of controllability works by using the second and forth quadrants, the overall power request is high compared to the other system suspensions.

1.8 State of the art

Regenerative suspensions have been studied and proposed in the past decades for enhancing the dynamic performance and converting wasted heat energy into electricity. Since then, the number of publications related to this topic have skyrocket.

Zuo, in 2013 obtained with his theorical work a mean value around 100–400W available from the shock absorbers of a middle-sized vehicle at 96 km/h on the good which is class B and average class C roads [16]; on the road test of a compact vehicle, a 60W energy potential is estimated at 40 km/h speed on a campus road profile test [17].

Fig. 11 **Compact vehicle on Stony Brook campus road.** [17]

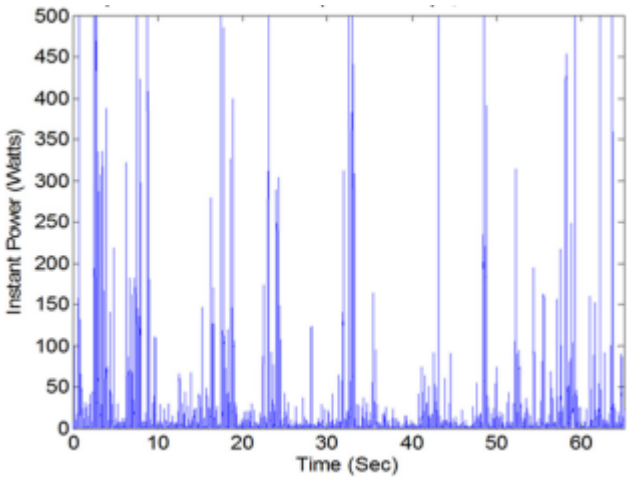

Fig. 12 **Energy dissipation in one shock absorber at 40 km/h, Rms = 14.6 W.** [17]

In this section there will be discussed the regenerative technologies; Electromagnetic linear harvesting shock absorbers, rotary mechanical transmission collecting energy shock absorbers, rotary hydraulic regenerative shock absorbers and the Audi eROT rotary harvester that inspires this work.

1.8.1 Regenerative Technologies

1.8.1.1 Electromagnetic linear harvesting shock absorbers

Basically, the linear-based electromagnetic damper works by transforming the energy which is kinetic by the vertical oscillations into electricity due to the electromagnetic induction with a structure that is simplistic in design. In the other hand the rotary electromagnetic harvesters that depend on a transmission to provide energy rotation to the electric motor with a motion that is unidirectional, in the linear system, a transmission mechanism is not required to generate the electricity, because the energy is generated due to vertical displacement. Because of this, electromagnetic harvester offers a high regenerative av power and the losses because of inertia, friction are by using transmissions are saved [18].

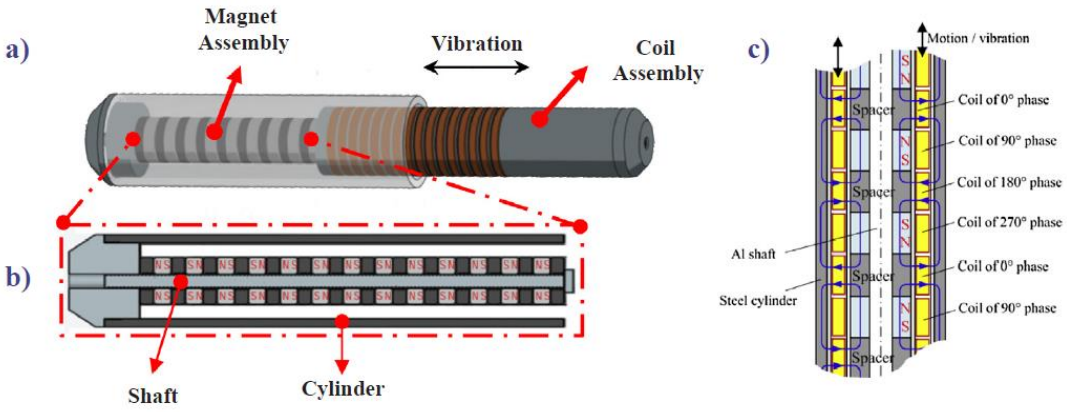

Fig. 13 **Linear electromagnetic shock absorber.** [17]

The road excitation caused by the road profile causes a movement that is linear translational of the magnet compared to the coil mounted in the device. This oscillating motion causes a magnetic flux variation inside the coil where the voltage is induced.

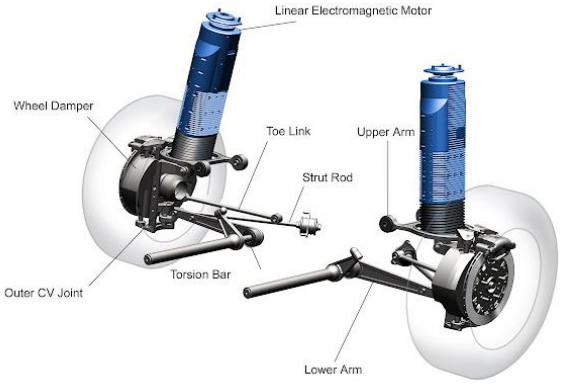

Fig. 14 **Bose suspension.** [19]

An example of this technology is the Bose suspension first developed in the 90s, with many magnets perfectly assembled and great size and weight, resulted in a very expensive device that didn't make it to the car factories.

1.8.1.2 Mechanical transmission based electromagnetic rotary harvesting shock absorbers

- **Rack pinion**

  The rack pinion consists of a rack where a pinion is mounted and moving according to the suspension excitation. Then it is connected to a small mechanisms similar to a differential that supplies rotational movement to the motor [23].

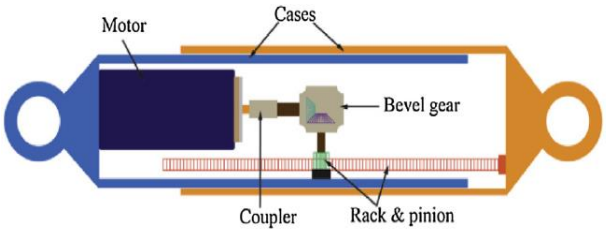

Fig. 15 **Rack pinion energy regeneration system.** *[21]*

For this technology there are no examples in the automotive industry

- **Ball screw**

The vibrations created due to the road conditions move a ball screw shaft that moves linearly according to the suspension excitations. A ball nut is fixed with balls inside for preventing backlash that makes the motor spin [21].

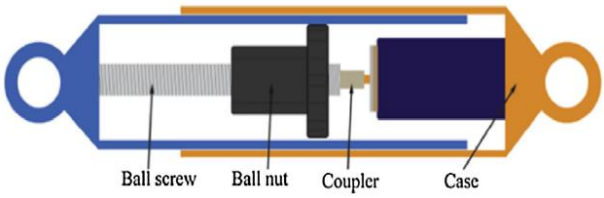

Fig. 16 **Ball screw energy regeneration system.** *[21]*

This technology was not implemented in the car industry, so there are no prototypes.

1.8.1.3 Modern commercial rotary energy harvesting technologies

- **Clear Motion**

The ClearMotion system is an Activalve, a software-centric electrohydraulic device that is situated on every corner of the vehicle, monitoring, processing, and responding to road conditions. The Activalve contains three main components the Gerotor, the BLDC Electric Motor and a digital controller. When the controller detects a disturbance, the Activalve is instructed to counteract by exacting pressure in the actuator body [23].

The Activalve is designed as part of the actuator body, it can be rotated or translated about the actuator axis to achieve fitment on the vehicle platform.

Active suspension master controller: real-time software that networks the 4X Activalves in the vehicle to execute active motion control. Data as collected by the integrated accelerometers at each corner is pushed through local vehicle telematics and ported to the cloud

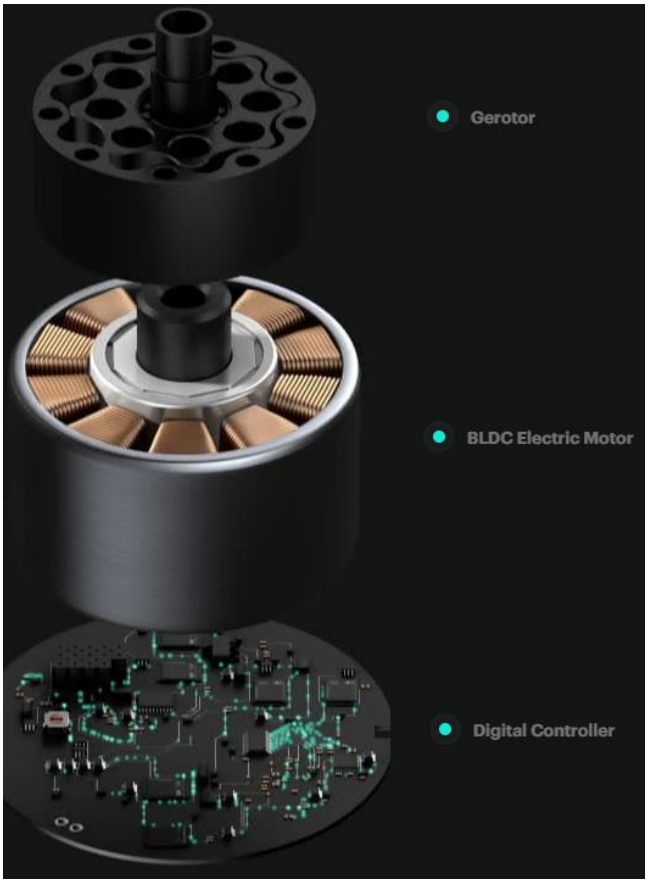

Fig. 17 **Clear Motion system with Active Valve.** [22]

- **Mechanical transmission based electromagnetic rotary without damper AUDI Erot**

  Audi has taken regenerative energy on suspensions into a new prototype called electromechanical rotary (eROT) suspension system that is designed to guarantee comfort ride and collect electricity at the same time [6].

  By electrically controlling the suspension Audi is able to separate a rebound and a compression, which means a compression soft damping and a rebound taut damping is feasible without the need of using vertical shock absorbers, which also clears up space in the suspension area.

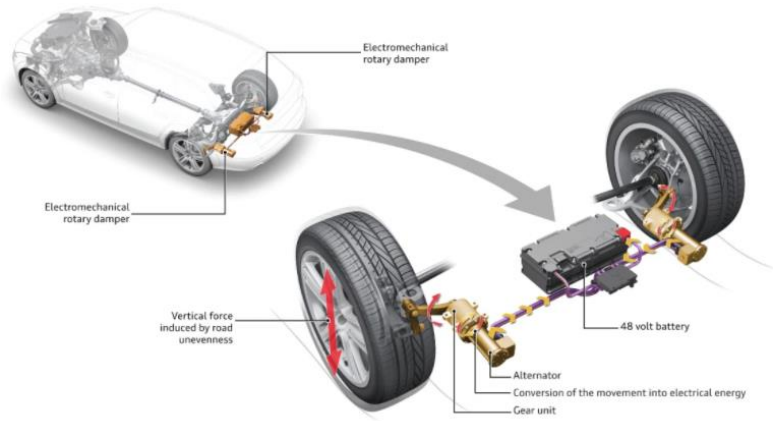

Fig. 18 **Erot system** [6]

The Audi eROT system can collect kinetic energy created by the oscillations of the road or bumps. The lever arms mounted on the suspension system are to absorb the wheel carrier movement, and then transmit that rotation motion to an electric motor through a gearbox to create electricity and store it in a battery pack [6].

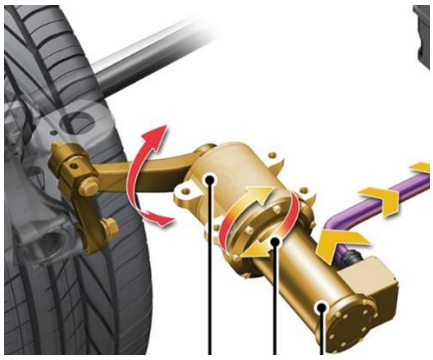

Fig. 19 **Erot lever and electric motor.** [6]

In average conditions, Audi states the system recuperates between 100-150 watts, but the results depend on the conditions of the terrain .On smooth roads like the billiard, it was able to create just 3 watts, and on difficult roads it returned up to 613 watts. Under average conditions in the city, the energy harvesting could mean savings of CO2 close to 3 g/km [6].

The mechanical rotary harvesters are better in terms of power harvested and conversion efficiency, so for this work continues with what the state of the art says which is a mechanical rotary harvester with no damper, but with the novelty of adding a cycloidal transmission that transform the vertical oscillations in a rotary motion that out puts a high speed rpm that goes in to the electric motor that finally will send it to a battery for storage and later use in other systems in the car.

1.8.2 Reasons for rotary electromechanical

According to Zuo's work, the mechanical harvester rotary transmission possess a efficiency in conversion that is superior to the rest of the motion transmission technologies [4].

Table 2 **Energy harvesting technologies comparison.** *[4]*

No.	Energy-Harvesting Technology	Linear-Rotary Motion Transmission	Harvestable Power Range (W)	Conversion Efficiency (%)
1.	Rotary electromagnetic energy-harvesting dampers (indirect-drive based electromagnetic harvesters)	Rack-Pinion Based Mechanism	20–250	30–70%
		Ball-Screw Based Mechanism	25–290	20–65%
		Hydraulic Based Mechanism	30–350	10–40%
2.	Linear electromagnetic energy-harvesting dampers (direct-drive based electromagnetic harvesters)	–	25–300	20–50%

The rack pinion mechanism is the one with best conversion efficiency for the harvested power it can take it is a reliable component because it is used on the direction system of the vehicle as well. Following is the ball screw mechanism with 5% less than the rack pinion, but totally depends on the metal balls it contains to work, and in third place the hydraulic mechanism which has the highest harvestable power, but low efficiency. It has plenty of draw backs, first its related to its size, because it contains plenty of components; a cylinder, a release Valve, a motor, a coupling, and a generator, which together are not capable no fit in most of car vehicles and because of its weight can interfere with the vehicle dynamics. Other problem is the system itself due to if there is a leakage the whole systems fail and affecting the comfort and response to the road severely.

As can be seen in Table 3 the linear electromagnetic energy provides a lower conversion efficiency up to 50% because of the large power loss during this system, but nonetheless it has a great harvestable power range. The draw back for this technology are that the tolerances must be very precise, otherwise the magnets and coils could be damaged, and this makes it expensive to construct or produce.

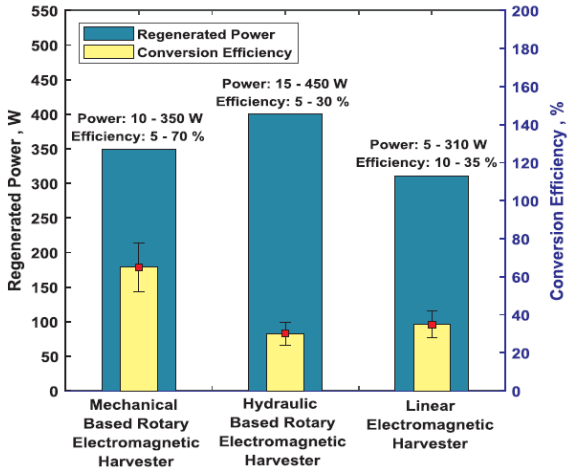

Fig. 20 **Conversion efficiency and regenerated power for different technologies** *[4]*.

In a summary, the tables provided are showing a tendency for the rotary mechanical energy collectors compared to the other two harvesters because the rotary mechanical are more simple for capturing the excitation energy, meanwhile in vehicles, the vibration harvest systems are considered an extra system where the harvest of power is not the only purpose, but it provides an acceptable performance talking about the performance indexes; road holding, ride handling compared to the state of the art in supensions.

2 Performance indexes and road profile

In this chapter are presented the model equations for a quarter car of the vehicle, the performance indexes, Comfort, handling, and power recovery. The ISO Road profiles and Road Roughness Model to synthetize road conditions. Simulations using different types of road classes with the EV-TEC vehicle parameters. Finally, simulations using an active actuator instead of the regular damper with two different strategies Sky hook and Ground hook.

2.1 Quarter car

The base model for this work is a quarter car modeled as a two degree of freedom. For practicity, the model is the simplest model of a vehicle's suspension, it consists of a suspension stiffness k2, a damping coefficient c2, tire stiffness k, a wheel mass m1 and a car mass m2 [4].

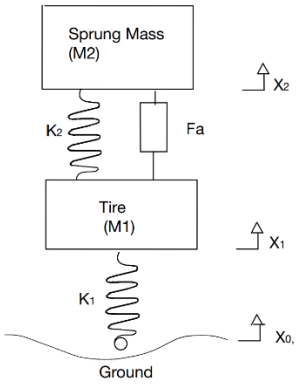

Fig. 21 **Quarter car model.** [17]

The Dynamic equations for this quarter car can be written as follows:

$$\bar{x} = A\bar{z} + B\bar{u}$$

$$\begin{bmatrix} \dot{X}_1 \\ \dot{X}_2 \\ \ddot{X}_1 \\ \ddot{X}_2 \end{bmatrix} = \begin{bmatrix} 0 & 0 & 1 & 0 \\ 0 & 0 & 0 & 1 \\ (-\frac{k_2}{m_1} - \frac{k_1}{m_1}) & \frac{k_2}{m_1} & -\frac{c_2}{m_1} & \frac{c_2}{m_1} \\ \frac{k_2}{m_2} & -\frac{k_2}{m_2} & \frac{c_2}{m_2} & -\frac{c_2}{m_2} \end{bmatrix} \cdot \begin{bmatrix} X_1 \\ X_2 \\ \dot{X}_1 \\ \dot{X}_2 \end{bmatrix} + \begin{bmatrix} 0 \\ 0 \\ \frac{k_1}{m_1} \\ 0 \end{bmatrix} \cdot [X_0] \quad (2)$$

$$\bar{y} = C\bar{z} + D\bar{u}$$

$$\begin{bmatrix} X_1 - X_2 \\ \dot{X}_2 - \dot{X}_1 \\ k_1(X_1 - X_0) \\ \ddot{X}_2 \end{bmatrix} = \begin{bmatrix} 1 & -1 & 0 & 0 \\ 0 & 0 & -1 & 1 \\ k_1 & 0 & 0 & 0 \\ \frac{k_2}{m_2} & -\frac{k_2}{m_2} & \frac{c_2}{m_2} & -\frac{c_2}{m_2} \end{bmatrix} \cdot \begin{bmatrix} X_1 \\ X_2 \\ \dot{X}_1 \\ \dot{X}_2 \end{bmatrix} + \begin{bmatrix} 0 \\ 0 \\ -k_1 \\ 0 \end{bmatrix} \cdot [X_0]$$

2.2 Comfort, handling, and power recovery

In this section the performance indexes are introduced, these indexes are very important to determine the passenger comfort, the security of the car in terms of handling and the average power which feedbacks the amount of energy recovered.

2.2.1 Comfort

To measure comfort is complex task, but nonetheless several studies have shown that human perception depends on the level of acceleration, direction, frequency, and location. The ISO 2631 standard mentions an evaluation method of the exposure effect to vibration on humans' body by using the root mean square acceleration with curves of human vibration-sensitivity [23].

Comfort is very important; it determines the preferences of people for certain cars. The least the sprung mass moves benefits more the comfort of the passengers in the cabin [24].

2.2.2 Handling

Road handling is a very important performance index. It depends on the static and dynamic contact force between the ground and tire. When there are a lot of vibrations the tires tend to lose ground contact which means losing control of the car and a dangerous situation. At dynamic force that is higher, the vehicle is not able to be handled safely on the road. The wheel lose contact with the terrain when the ratio is equal or over 1 of dynamic and static contact forces. Thus, the road handling (3) performance index can be defined as the ratio that is between the dynamic loads to static loads [17].

$$\eta_{rs} = \frac{k_1 \cdot (x_1 - x_0)}{(m_1 + m_2) \cdot g} \tag{3}$$

Handling is crucial, it needs to be perfect in order to have a total control of the car while driving and to avoid accidents.

2.2.3 Power Recovery

The available max energy that is for collecting is the same energy that is dissipated by the c_2 viscous damping. The suspension velocity is proportional to the instant damping force, and the instant power is the force times the suspension velocity. Therefore, the instant power dissipation is (4). The shock absorber average power is proportional to the mean square of the velocity suspension. Power collecting over this among will yield a damping coefficient with the suspension more than the target value [17].

$$P = c_2 \cdot (\dot{X}_2 - \dot{X}_1)^2 \tag{4}$$

Power recovery is fundamental because it is what makes the suspension in to capable of harvesting energy from the vertical oscillations of the car.

2.3 ISO road profiles

The disturbance of road displacement input is modeled as white noise input, it goes into low pass filter called $H_{road}(s)$ that produces the road behavior. The road class can be modified by changing the Gr to represent different road conditions in the equation (5). The wheels on the road follow the terrain profile X_0 which is the main input for the vehicle vibrations. The vehicle modeling equations are obtained with the quarter car analysis.The out puts are the weighted acceleration, the displacement, velocity and tire / ground contact force.

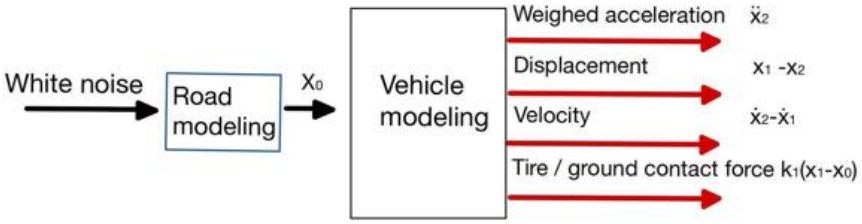

Fig. 22 **Block diagram of vehicle dynamics** [3]**.**

$$H_{road}(s) = \frac{2 * \pi \cdot \sqrt{Gr \cdot v}}{s + w_{cut}} \tag{5}$$

In the equation (5) Gr is the geometric road, v is the var velocity, w_{cut} is the cut frequency

2.3.1 Road Roughness Model

To classify the roughness of a road surface, this work is based on the International Organization for Standardization (ISO 8606). The ISO offers a road roughness classification using the PSD values (ISO, 1982), as shown in Table 4.

Table 3 **Road roughness values classified by ISO 8606.** [8]

$\boldsymbol{Class}$	$\boldsymbol{Gr(m^2\ cycles/m)}$
A	1.6×10^{-7}
B	6.4×10^{-7}
C	2.56×10^{-6}
D	1.024×10^{-5}
E	4.096×10^{-5}
F	1.6384×10^{-4}
G	2.62×10^{-4}

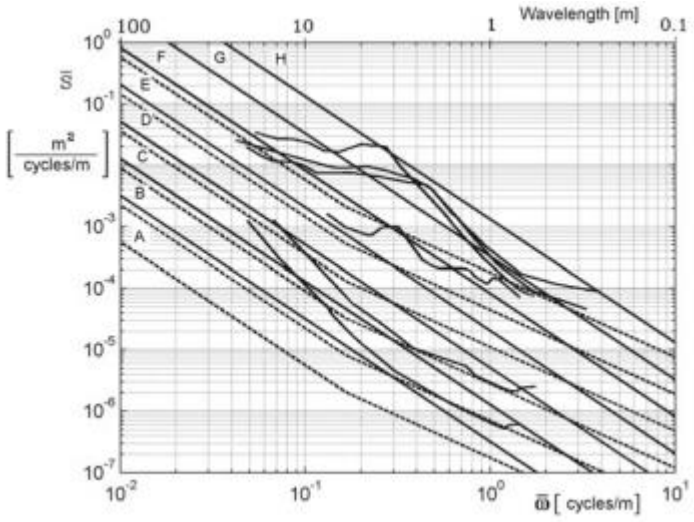

Fig. 23 **Power spectral density of some road profiles ISO 8606:1995 standard (full lines).** *[8]*

The road class that will be selected for this work will be a Road class type C which is the average road condition in Mexico, also a Road class type B is performed to compare the impact of road condition on performance indexes.

2.4 Sensitivity to damping.

The quarter car space matrices obtained in the previous section are used to perform two simulations where c_2 varying and the road condition was synthetized according to table 3 and the low pass filter (Road modeling) with a road class C.

The parameters to perform the simulations are from the EVTEC vehicle, developed in the past years by students and professors from the Tec de Monterrey (ITESM) [22].

Fig. 24 **EV TEC** [22].

The parameters for the EV TEC are:

Parameters

- Sprung mass 247.5 kg = m_2
- Unsprung mass 38 kg = m_1
- Suspension stiffness 14070.1 N/m = k_2
- Tire stiffness 323470 N/m = k_1

The suspension stiffness is the value of the vertical reaction of the vehicle, but to obtain the real suspension stiffness it can be calculated as follows:

$F_A = Force\ on\ the\ tire$
$K_s = Suspension\ stiffness$
$\alpha = Angle\ between\ shock\ absorber\ and\ lower\ arm$
$d_s = Distance\ from\ spring\ centreline\ to\ the\ control\ arm\ inner\ pivot\ center$
$d_a = Distance\ from\ wheel\ to\ the\ control\ arm\ inner\ pivot\ center$

$q_a = Displacement\ of\ the\ suspension\ vertically\ at\ the\ wheel$

$$F_A = \frac{K_S}{sin^2\alpha} \cdot \left(\frac{d_s}{d_a}\right)^2 \cdot q_a \tag{6}$$

$$\frac{F_A \cdot sin^2\alpha}{q_a \cdot \left(\frac{d_s}{d_a}\right)^2} = K_S$$

In the next sections the simulations results are presented for road classes C and B for a passive suspension.

2.4.1 Road class B

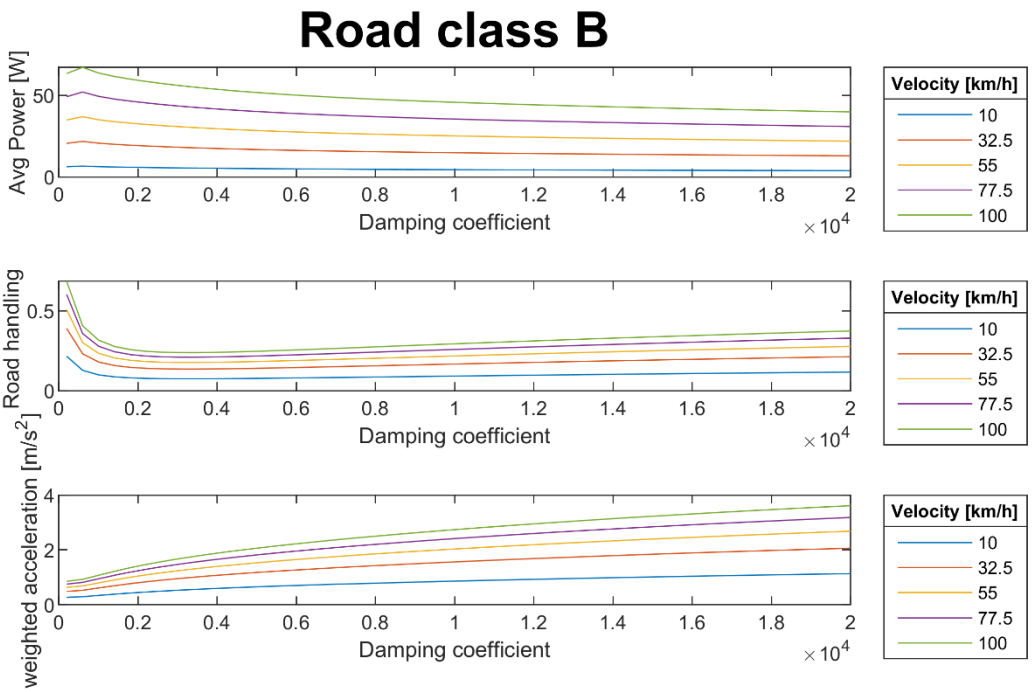

Fig. 25 **Avg power, road handling and weighted acceleration for road class B.**

In the first graph as the velocity and damping coefficient increases in a Road class B the average power barely changes. It can be understood that as the stiffer the damping is, less the suspension moves and therefore the velocity is minimal and that is why the power does not vary much.

In the second graph, road handling goes down and starts to rise slightly as damping increases. The same pattern can be seen as velocity increases. Road handling can drop twice or more as the damping increases. Seems like the perfect point for this car in all velocities is around 2000Ns/m because is the lowest point, which means great ground contact.

In the third graph, the weighted acceleration decreases as the damping coefficient increases. The same pattern happens at different velocities. Can be concluded that the damping coefficient affects comfort because weighted acceleration almost triple decreased as the damping gets a higher value.

2.4.2 Road class C

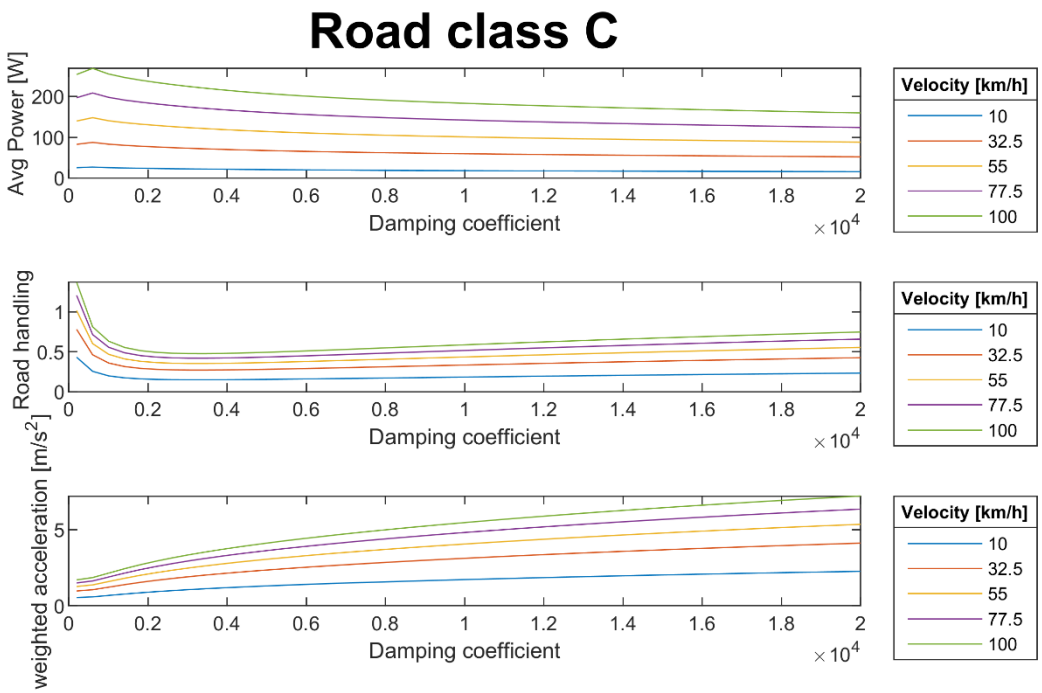

Fig. 26 **Avg power, road handling and weighted acceleration for road class C**.

In the first graph as the velocity and damping coefficient increases in a Road class C the average power barely changes. It can be understood that as the stiffer the damping is, less the suspension moves and therefore the velocity is minimal and that is why the power does not vary much.

In the second graph, road handling goes down and starts to rise slightly as damping increases. The same pattern can be seen as velocity increases. Road handling can drop twice or more as the damping increases. Seems like the perfect point for this car in all velocities is around 2200 Ns/m because is the lowest point, which means great ground contact.

In the third graph, the weighted acceleration decreases as the damping coefficient increases. The same pattern happens at different velocities. Can be concluded that the damping coefficient affects comfort because weighted acceleration almost triple decreased as the damping gets a higher value.

In summary in a semi active suspension according to the two previous simulations what can only be achieved is varying the damping, which is what all car manufactures do nowadays. This statement is

reinforced since Weighted acceleration (comfort) is greatly affected when damping varies compared to the impact of damping varying in road handling and average power.

2.5 Active strategies (Skyhook/Groundhook)

In this section the concepts of Skyhook, Groundhook and a brief explanation o why active suspensions are presented. The first one is mainly for comfort and the second for better handling. Next two simulations are performed for Skyhook where c_{sky} is varying and the road condition was synthetized according to table 3 and the low pass filter with a road class C. Same situation for the ground hook where c_g is varying and the road condition was synthetized according to table 3 and the low pass filter with a road class C. Finally, two more simulations are presented at 35 km/h with the behavior for the Skyhook and Groundhook.

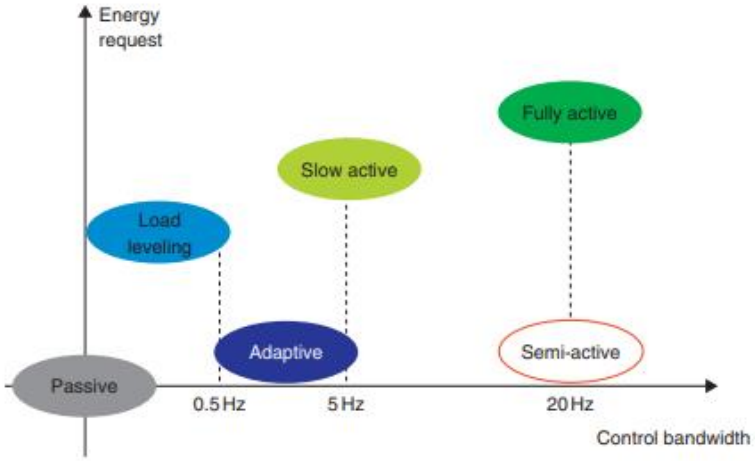

Fig. 27 **Suspension system classification** [9]**.**

The reason for using active strategies is because of the controllability range is better that the other systems as can be shown in fig 27. Active suspensions have a quicker response of milliseconds and if they are regenerative active suspensions, they have a demand in energy that is lower than a regular fully active which makes them attractive than other types of suspension systems [9].

2.5.1 Skyhook

The Skyhook consists of a passive damper that is ideal, and it is connected between the sprung mass and an imaginary position in the space. This configuration has beneficial effects when mitigating the resonance that comes from the road conditions and improves an isolation when the Skyhook damping ratio value is increased, contrary to passive suspensions systems a resonant transmissibility is enhanced when the passive damping is increased, but as a drawback the high frequency isolation performance is decreased [9]. In the other hand in a Skyhook damper configuration, the damper

force is in function of the absolute velocity of the sprung mass and the Skyhook damper provides damping without transmitting the unsprung mass vibrations to the whole body because it is not connected to the unsprung mass. The imaginary fix point where the Skyhook damper is positioned to maintain steady the sprung mass does not exist, so as a consequence this configuration strategy needs to be implemented using an actuator located between the sprung and the unsprung masses like in fig 27.

If the damping coefficient c_{sky} has a positive value, means it dissipates energy, like a passive damper, but when c_{sky} has a negative value, the damper is introducing energy into the system, with an actuator [12].

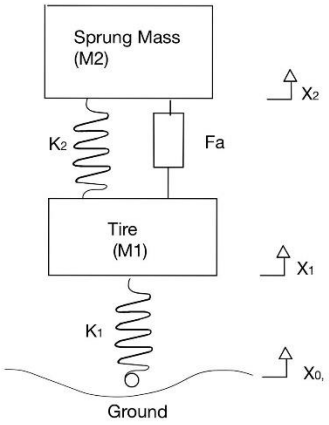

Fig. 28 **Quarter car with actuator for Skyhook strategy.**

Based on the modified quarter car new space matrices are created, an actuator Fa (6) is placed instead of the regular damper system with a varying c_{sky} while c_2 has fixed value.

$$F_a = -c_{sky} \cdot \dot{X}_2 - c_2 \cdot (\dot{X}_2 - \dot{X}_1) \tag{7}$$

The power convention for the simulation plots of the active strategies is positive (+) when the actuator delivers energy and negative (-) when the actuator is dissipating energy for both, the Skyhook and Groundhook.

Next the space matrices are presented:

$$\bar{x} = A\bar{z} + B\bar{u}$$

$$\begin{bmatrix} \dot{X}_1 \\ \dot{X}_2 \\ \ddot{X}_1 \\ \ddot{X}_2 \end{bmatrix} = \begin{bmatrix} 0 & 0 & 1 & 0 \\ 0 & 0 & 0 & 1 \\ (-\frac{k_2}{m_1} - \frac{k_1}{m_1}) & \frac{k_2}{m_1} & 0 & 0 \\ \frac{k_2}{m_2} & -\frac{k_2}{m_2} & 0 & 0 \end{bmatrix} \cdot \begin{bmatrix} X_1 \\ X_2 \\ \dot{X}_1 \\ \dot{X}_2 \end{bmatrix} + \begin{bmatrix} 0 & 0 \\ 0 & 0 \\ \frac{k_1}{m_1} & -\frac{1}{m1} \\ 0 & \frac{1}{m_2} \end{bmatrix} \cdot \begin{bmatrix} X_0 \\ Fa \end{bmatrix} \quad (8)$$

$$\bar{y} = C\bar{z} + D\bar{u}$$

$$\begin{bmatrix} X_1 - X_2 \\ \dot{X}_2 - \dot{X}_1 \\ k_1(X_1 - X_0) \\ \ddot{X}_2 \\ \dot{X}_1 \end{bmatrix} = \begin{bmatrix} 1 & -1 & 0 & 0 \\ 0 & 0 & -1 & 1 \\ k_1 & 0 & 0 & 0 \\ \frac{k_2}{m_2} & -\frac{k_2}{m_2} & 0 & 0 \\ 0 & 0 & 0 & 1 \end{bmatrix} \cdot \begin{bmatrix} X_1 \\ X_2 \\ \dot{X}_1 \\ \dot{X}_2 \end{bmatrix} + \begin{bmatrix} 0 & 0 \\ 0 & 0 \\ -k_1 & 0 \\ 0 & \frac{1}{m_2} \\ 0 & 0 \end{bmatrix} \cdot \begin{bmatrix} X_0 \\ Fa \end{bmatrix}$$

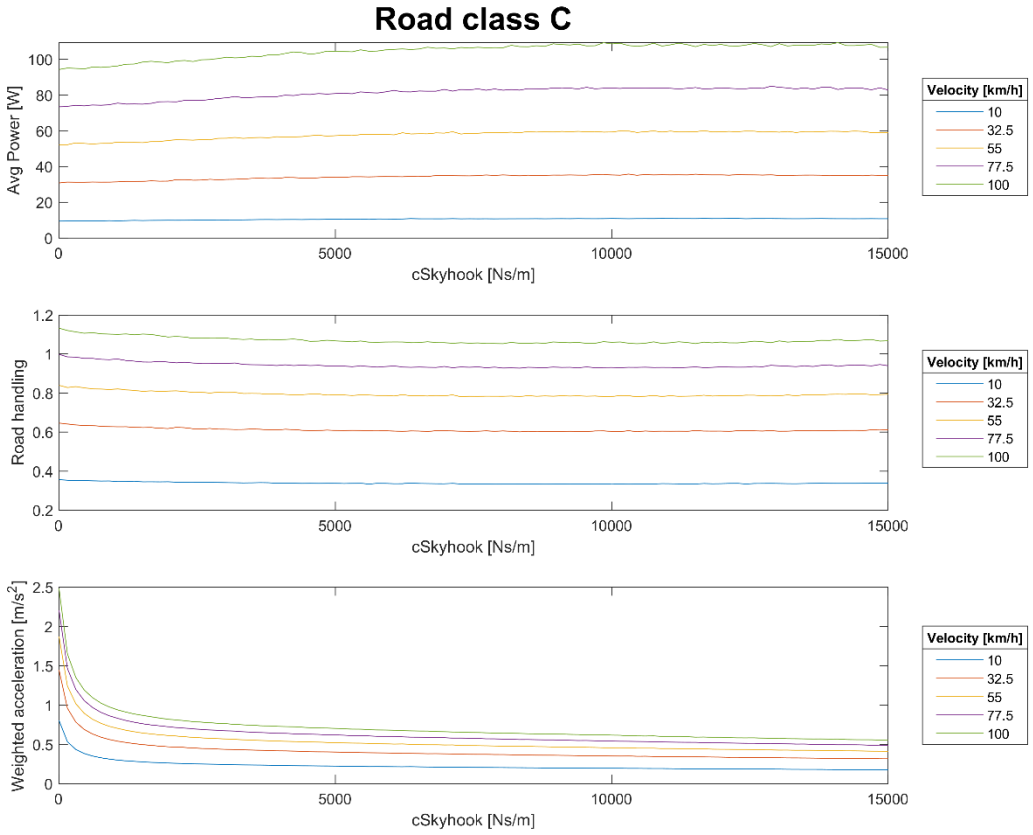

Fig. 29 **Avg power, road handling and weighted acceleration varying Skyhook for road class C.**

In the first graph the average power slightly increases as the c_{sky} is increasing.

The road handling around 0.6 and 0.8 has its best value, which is the lowest point, but then it starts to increase and losing ground contact when it goes over 1 while c_{sky} is increasing.

The Weighted acceleration is reduced while c_{sky} is increasing which means a less acceleration in the vehicle. Compared to the simulation performed in the previous chapter an improvement in comfort is achieved with the Skyhook.

Can be observed that road handling and weighted acceleration have an opposite behavior. While one goes up and get worst, the other goes down and improves.

For a better understanding on Fig 28. using the Skyhook configuration, can be seen in which scenarios, the suspension behaves like a damper and as actuator.

The system tends to behave more as a damper. As can be seen the suspension occupies all the quadrants which indicates that there are great opportunities to use an active control for the suspension.

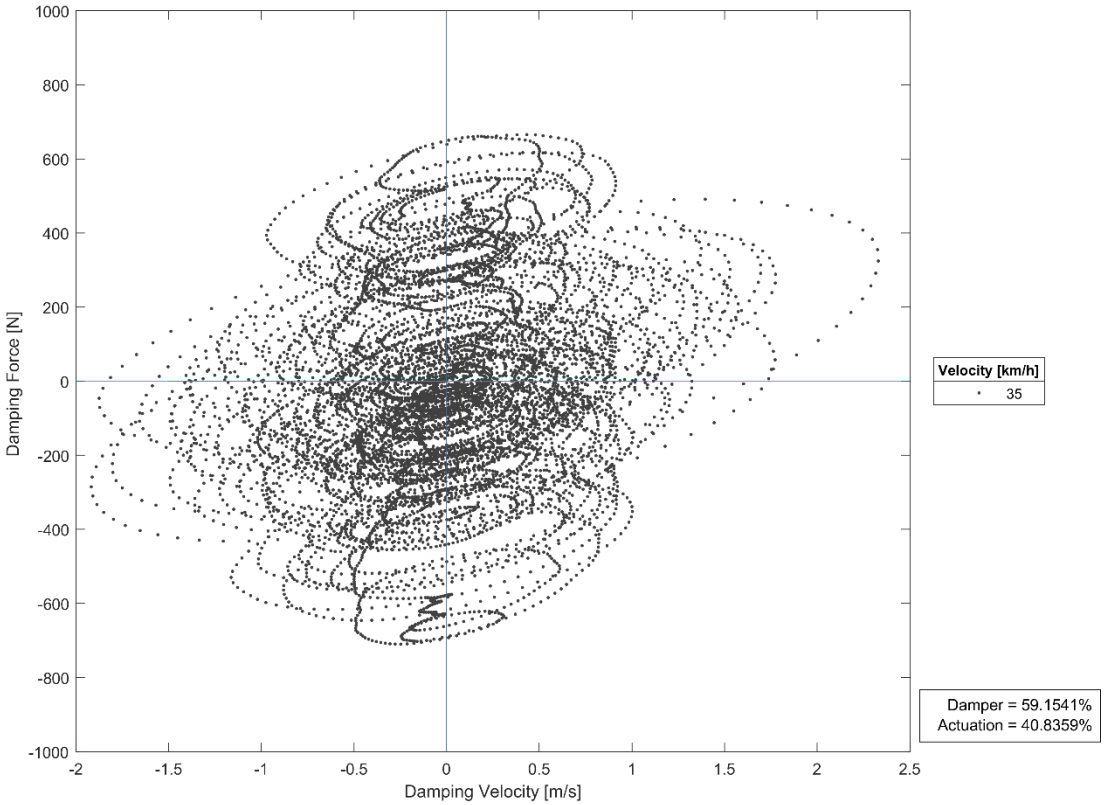

Fig. 30 **Damper and Actuation response with skyhook.**

2.5.2 GroundHook

The Groundhook control is a modified version of the Skyhook damper is a configuration where the damper is connected to $M1$ which for this work is the unsprung mass rather than $M2$ that corresponds to the sprung mass [9]. This configuration is called Groundhook. The Groundhook configuration system is kind of similar to the response of the Skyhook damper configuration, with the mainly difference that the Groundhook configuration adds more damping to the unsprung mass and removes it from the sprung mass. This approach is ideal and in practice it is performed using only with the F_a actuator where an active or semi-active device is located between the two masses. If an active system is used, the force exerted on the unsprung mass is as follows:

$$F_a = -c_g \cdot \dot{X}_1 \tag{9}$$

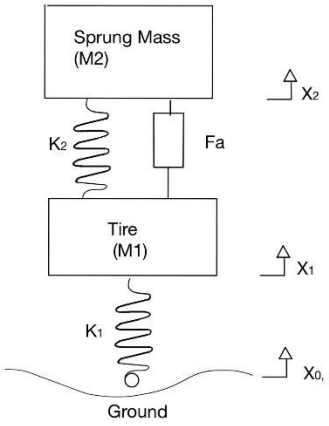

Fig. 31 **Quarter car with actuator for Ground hook strategy.**

Based on the modified quarter car new space matrices are created, an actuator Fa is placed instead of the regular damper system with a varying c_g (cGroundhook) while c_2 has fixed value.

Next the space matrices are presented:

$$\bar{x} = A\bar{z} + B\bar{u}$$

$$\begin{bmatrix} \dot{X}_1 \\ \dot{X}_2 \\ \ddot{X}_1 \\ \ddot{X}_2 \end{bmatrix} = \begin{bmatrix} 0 & 0 & 1 & 0 \\ 0 & 0 & 0 & 1 \\ (-\frac{k_2}{m_1} - \frac{k_1}{m_1}) & \frac{k_2}{m_1} & 0 & 0 \\ \frac{k_2}{m_2} & -\frac{k_2}{m_2} & 0 & 0 \end{bmatrix} \cdot \begin{bmatrix} X_1 \\ X_2 \\ \dot{X}_1 \\ \dot{X}_2 \end{bmatrix} + \begin{bmatrix} 0 & 0 \\ 0 & 0 \\ \frac{k_1}{m_1} & -\frac{1}{m1} \\ 0 & \frac{1}{m_2} \end{bmatrix} \cdot \begin{bmatrix} X_0 \\ Fa \end{bmatrix} \quad (9)$$

$$\bar{y} = C\bar{z} + D\bar{u}$$

$$\begin{bmatrix} X_1 - X_2 \\ \dot{X}_2 - \dot{X}_1 \\ k_1(X_1 - X_0) \\ \ddot{X}_2 \\ \dot{X}_1 \end{bmatrix} = \begin{bmatrix} 1 & -1 & 0 & 0 \\ 0 & 0 & -1 & 1 \\ k_1 & 0 & 0 & 0 \\ \frac{k_2}{m_2} & -\frac{k_2}{m_2} & 0 & 0 \\ 0 & 0 & 1 & 0 \end{bmatrix} \cdot \begin{bmatrix} X_1 \\ X_2 \\ \dot{X}_1 \\ \dot{X}_2 \end{bmatrix} + \begin{bmatrix} 0 & 0 \\ 0 & 0 \\ -k_1 & 0 \\ 0 & \frac{1}{m_2} \\ 0 & 0 \end{bmatrix} \cdot \begin{bmatrix} X_0 \\ Fa \end{bmatrix}$$

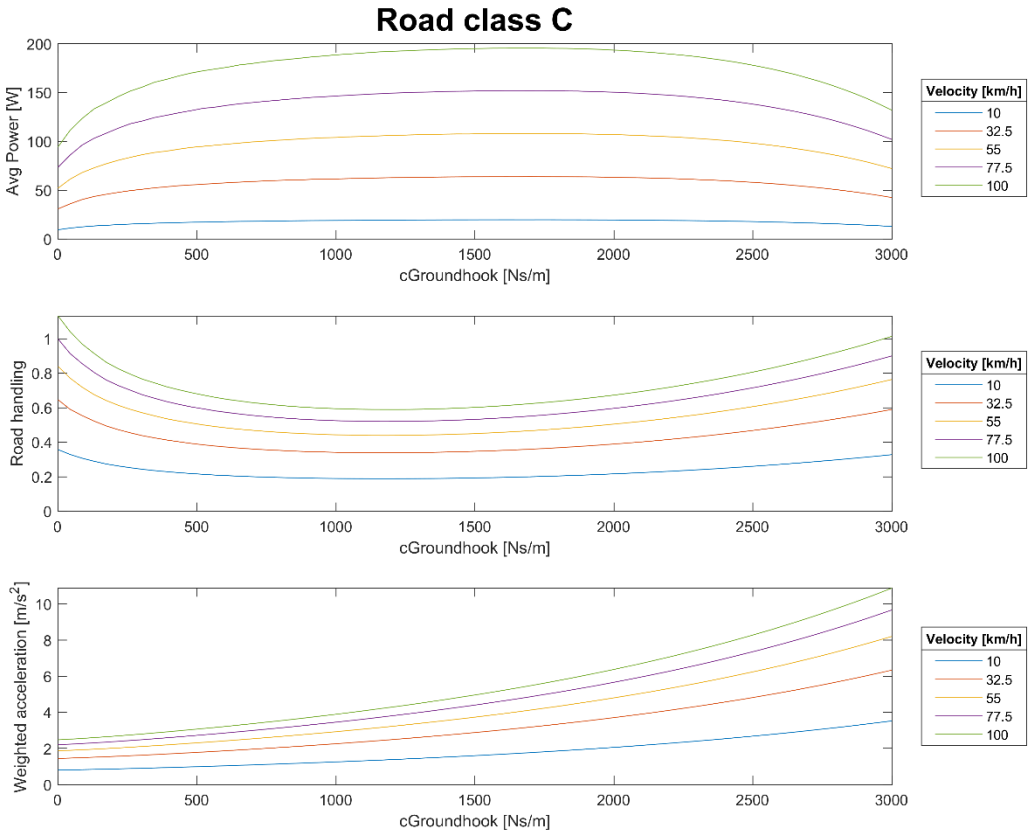

Fig. 32 **Avg power, road handling and acceleration varying cGgroundhook for road class C** [3].

The average power increases significantly while the c_g increase its value. Also notice as the velocity increases the power obtained goes up.

The Road handling while c_g is varying has an optimal point around 1000 Ns/m where at different speeds is less than 1 which means that the vehicle has a great ground contact. Compared to the simulation performed in the previous chapter an improvement in road handling is achieved with the Groundhook configuration.

The weighted acceleration keeps increasing as the c_g goes up which means less comfort. Notice that the road handling and weighted acceleration have an opposite behavior.

For a better understanding on Fig.31 using the ground hook configuration, can be seen in which scenarios, the suspension behaves like a damper and as actuator.

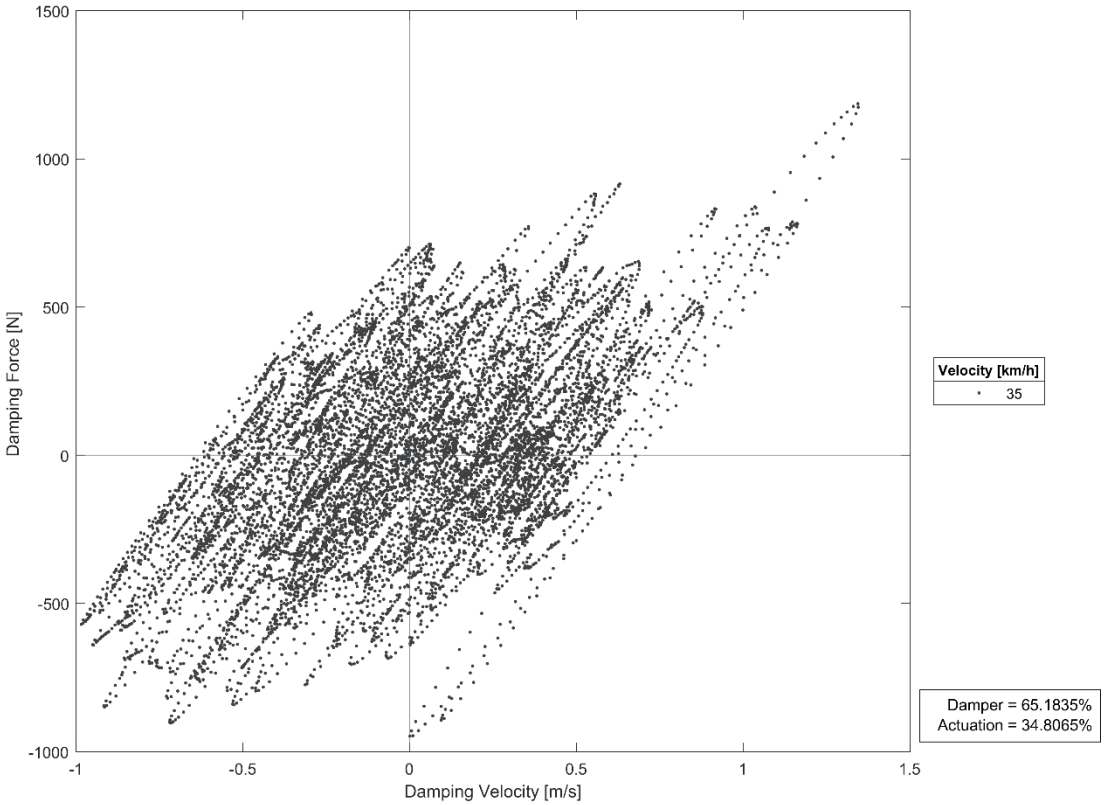

Fig. 33 **Damper and Actuation response with Groundhook**. [6]

The system tends to behave more as a damper. As can be seen the suspension occupies all the quadrants which indicates that there are great opportunities to use an active control for the suspension.

Table 4 **Comparative Chart of Working cycle**

WORK CYCLE		
Velocity of 35[$\frac{km}{h}$]	**Damper/regenerative [%]**	**Actuation [%]**
Skyhook	59.2	40.8
Groundhook	65.2	34.8

Can be concluded in table 4 that the Skyhook configuration works more in the active area, because it behaves more as a system that compensates the spring movement and doing that task requires more active power. The Groundhook dissipates more power, but in order to harvest that energy there are other factors that need to be taken in to account like the actuator limit capabilities.

Table 5 **Comparative Chart.**

Speed 35[$\frac{km}{h}$]	**Damping coefficient [$\frac{Ns}{m}$]**	**Average power [W]**	**Road handling**	**Weighted acceleration [$\frac{m}{s^2}$]**
Passive suspension	(Best handling) 3029	73	0.27	1.91
	(Best comfort) 604	88	0.46	1.1
	cSkyhook coefficient [$\frac{Ns}{m}$]			
Skyhook configuration	(Best comfort) 15000	35	0.61	0.3
	cGroundhook coefficient [$\frac{Ns}{m}$]			
Groundhook configuration	(Best handling) 1174	63	0.34	2.46

In table 5 can be appreciated that at 35 km/h for the passive suspension there is not a common point where the road handling and comfort are optimal notice that the damping coefficient is different for best handling and best comfort. At 0.27 is the best handling, the lower this value is the better performance in handling is obtained, for weighted acceleration 1.1[$\frac{m}{s^2}$] is the lowest value which means less acceleration of the sprung mass and therefore better comfort.

For Skyhook strategy which is mainly for comfort improvement the lower the cSkyhook damping coefficient is the best comfort is obtained, because this strategy consists of maintaining the sprung mass steady with active force.

For Groundhook strategy the main task is to achieve the best handling which is the lowest value by connecting the unsprung mass to the ground.

2.6 Bode diagrams for comfort and handling

There are two signals that are used for the bode diagrams, the acceleration of the sprung mass that is related to comfort and the road handling that is for ground contact. These signals are compared against the terrain X_0 to obtain the bode diagrams. In the frequency domain the plot of the response of the system can be observed at different frequencies.

The first peak is a response to the suspension itself and the second peak is the resonance frequency of the tire.

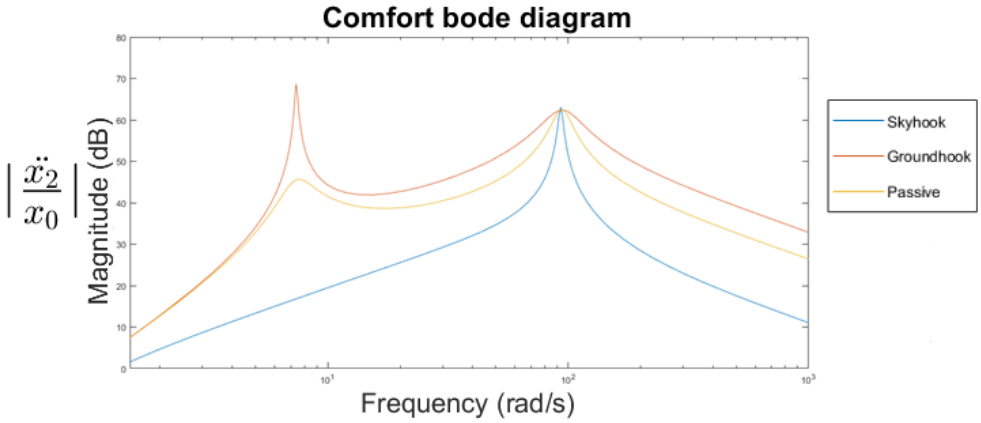

Fig. 34 **Bode diagram for comfort.**

Fig 34. presents the comparison of the acceleration against the road profile can be observed that for Skyhook the first peak is attenuated, which is a characteristic for this configuration enhancing comfort, while for Groundhook the first peak has increased because it is mainly for road handling, being the second peak softer than the other two when reaching the resonance point.

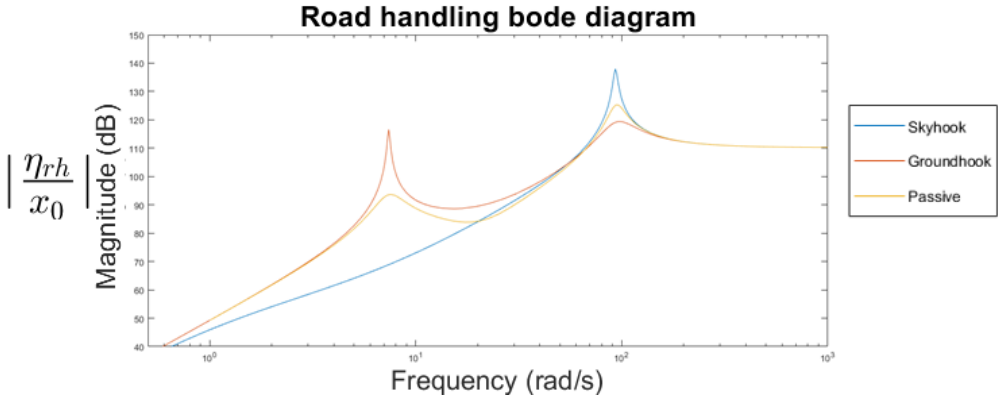

Fig. 35 **Bode diagram for road handling.**

Figure 35. is about the comparison of the road handling performance index versus the road profile.

The Skyhook configuration has a worse behavior compared to the other two, and the Groundhook configuration has an improvement in the second peak with softer resonance point. It's important

to notice that the sprung mass is oscillating a lot for Groundhook, because there it tends to oscillate because the actuator in maintaining steady the unsprung mass.

The speed of the car combined to the road profile can create an excitation that is very close to the resonance of the car. A bump doesn't matter when reaching the resonance peak, the most important is the frequency of the excitations, because very small bumps can produce large vertical acceleration in the chassis. Analysis in the frequency domain add a very important dimension to the observation to the system responses.

3 Design Methodology

On this chapter first the methodology is explained to get from the vertical oscillations of the suspension to the Electric Motor torque. Next, the gearbox that best fits for energy harvesting is selected. Once the transmission is selected its position in the rear suspension is defined. Then, the gearbox and electric motor model is proposed and finally a multivariable optimization strategy is used to obtain the best values for the volume of the system.

3.1 Methodology for the design

First, its fundamental to understand that the vertical oscillations of the suspension are converted in to rotational for the transmission to then transform that high tor que input into more speed and less torque for the electric motor.

The force and velocity that comes from the suspension oscillations are values needed to be determined, both vary depending on the type of car and suspension.

The suspension transmission ratio (τ_1) can be obtained from the slope of the wheel vertical linear displacement (z_w) versus the angular displacement (α_{sd}) of the control arms.

$$\tau_1 = \frac{\alpha_{sd}}{z_w} \tag{10}$$

The angular speed (ω_s) can be determined with the speed (S_p) of the suspension and the suspension transmission ratio.

$$\omega_s = \frac{S_p}{\tau_1} \tag{11}$$

Next, the Torque of the gearbox (T_g) can be determined which is the force of the suspension times the suspension transmission ratio.

$$T_g = F \cdot \tau_1 \tag{12}$$

Following, the Torque of the electric motor (T_m) is determined as the Torque of the gearbox times the gearbox ratio (τ_g).

$$T_m = T_g \cdot \tau_g \tag{13}$$

All these steps are very important to then connect both the transmission and electric motor model for the optimization of the volume.

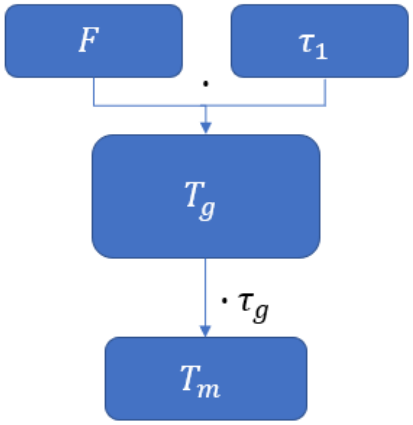

Fig. 37 **Target Torque motor**.

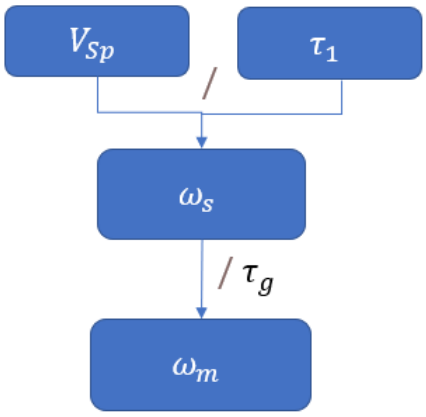

Fig. 36 **Angular velocity motor**.

This is a way to determine the target Electric Motor torque, but there is also an analytical option and one with finite elements.

3.2 Gearbox selection (harmonic vs planetary vs parallel axes vs cycloid drives)

The purpose of adding a gearbox before the electric motor is because, Electric Motors work better in different speeds which are high and low torque. For this work if the motor is attached directly in to one of the control arms it would experience a high torque with low speed input that may cause the motor to not work properly, so to satisfy the motor necessities a transmission needs to be the intermediate between the suspension rotational movement and the electric motor.

For this work the necessities for a gearbox are an input with high torque and an output of high speed that will be attached to an electric motor to maximize the energy harvesting. Since the gearbox and electric motor are going to be attached to any of the control arms affecting the vehicle dynamics. Therefore, to reduce the impact in the vehicle dynamics the volume should be minimized.

To select a proper transmission, scaling laws can be used to help the design satisfy the requirements for the project in terms of the size. The transmissions that are possible candidates for the project are 5: parallel shaft, planetary gear trains both multistage, harmonic drives heavy duty, cycloid drives more used in robotics, and ball screws that are common in direction systems. To compare the inertia and the maximum torque obtained for these 5 transmissions will be from the load side. The diameter, axial length, number of stage and the gearbox ratio are the main design functions for the scaling laws. [26].

Table 6 **Max torque and inertia for different transmissions** [27]**.**

These laws are made with the outer parameters of the transmission (diameter (d) and length (L), transmission ratio (i) and number of stages (a).

	Maximum continuous output torque	**Reflected inertia (to load side)**
Parallel Shaft Gear Train (PSGT)	$\frac{L \cdot d^2}{a}$	$\frac{L \cdot d^4 \cdot i^2}{a}$
Planetary Gear Train (PGT)	$\frac{L \cdot d^2}{a}$	$\frac{L \cdot d^4 \cdot i^2}{a}$
Harmonic Drive	d^3	$L \cdot d^4 \cdot i^2$
Cycloid Drive	$\frac{d^4}{L}$	$L \cdot d^4 \cdot i^2$
Ball Screw	d^3	$L \cdot d^4$

From Table 6 can be concluded that the diameter of the transmissions has a great influence when obtaining the maximum continuous output torque for all transmissions. In the other hand with the axial length seems like a negative influence or minimal is obtained. PGTs and PSGTs, there is an increase of a higher torque thanks to the length, but for the harmonic drive and ball screw in the scaling laws there is no effect caused by the axial length. About Cycloid drives, the length increase can cause several problems from failure in the pins to a diminish the continuous maximum output torque, because if the device has a cylindrical form and considerable length, the pins, cycloid gears will experience more contact force, which therefore increases the bending stresses creating a complicating scenario [26].

Observing the table 6 for the reflected inertia can be stated that the diameter of the transmissions has a great effect, due to the fact that it is d^4 while the axial length is L^1. Now, because torque and

inertia both have a conflict related to the diameter of the transmissions, the inertia of the gearbox candidates needs to be investigated in respect to the one of the motors. Usually, the inertia o the motor is what matters because it is the element at the end, so it as to deal with all the inertia of all the elements connected before [26].

From figure 34. can be concluded that harmonic drives have a high inertia compared to the cycloid drive and PGTs and the 2 motors especially the Maxon EC flat has a high inertia.

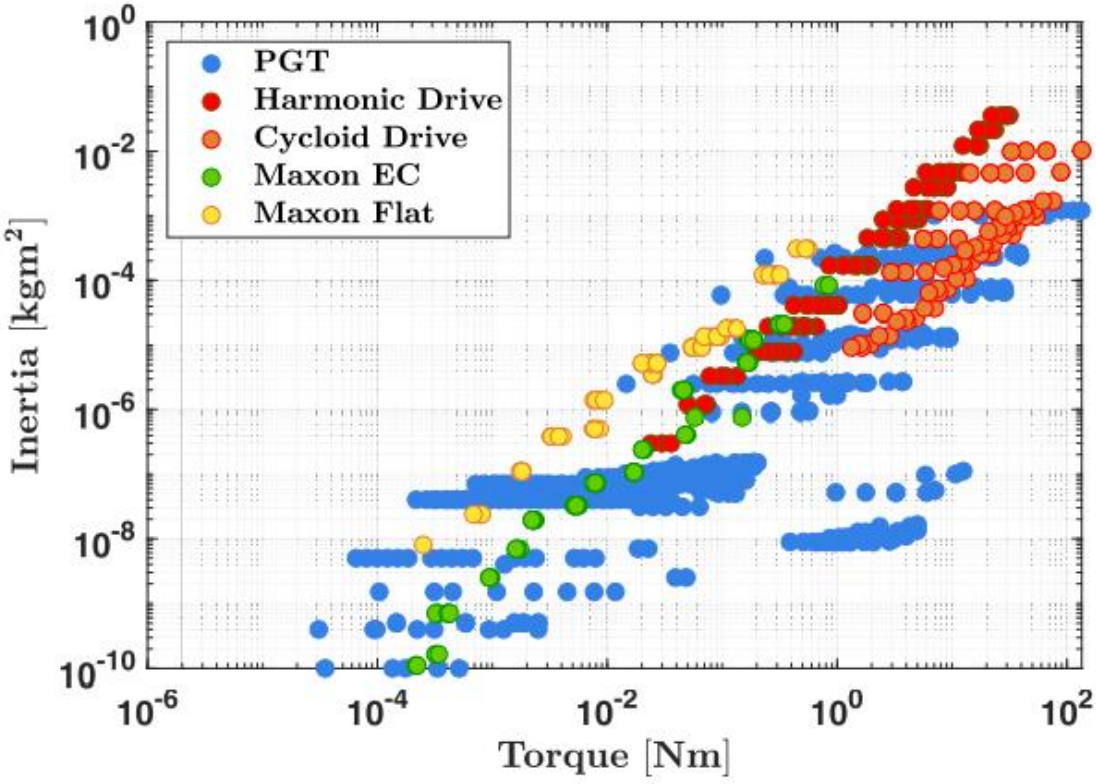

Fig. 38 **Inertia vs Torque for transmissions and electric motors** [31] [32] [33] [34] [35].

In conclusion the derived scaling laws show that:

- From the parameters which are the length L and the diameter d, the diameter is the principal factor for the torque and inertia.
- To obtain an optimized torque, a disc-shaped transmission gearbox is the most desired choice over a cylinder-shaped one otherwise it can cause interference.

- For inertia, it has conflicting demands in terms of diameter selection. A minimal diameter might be something desired for lowering the inertia, but it is not always crucial, since the inertia of the motor that is connected to the transmission, is usually more important when the inertia is investigated for the whole system
- The technology selected for this work is the cycloid drive, because it has a great dependency in the diameter d and is restricted by its length L which means a large transmission affects the torque and

the design for the transmission is forced to have a disc shape which perfectly fits for the project where a small device and high torque is needed. In terms of the inertia, it needs to be investigated to determine if it is relevant compared to the inertia of the motor.

The cycloid drive has a reduced volume as can be seen in this work, it is a great candidate to replace a regular shock absorber, but beside all its properties, friction is something that needs to be considered due to the fact that it creates a significant impact in the cycloid strength in the core [32]. There are several models to calculate the friction of the cycloid drive. In a study where the friction torque, contact force, efficiency and friction torque were calculated just between the cycloid pin gear and the cycloid gears shows that an increase in the coefficient of friction creates a rise in the contact forces and friction torque [32]. This friction torque is not desired because it reduces the efficiency and the increase in the contact forces affect the stress deformation of the components inside the cycloid drive. A more precise model needs to be developed in other to have a better understanding of the friction inside all the components of the cycloid drive.

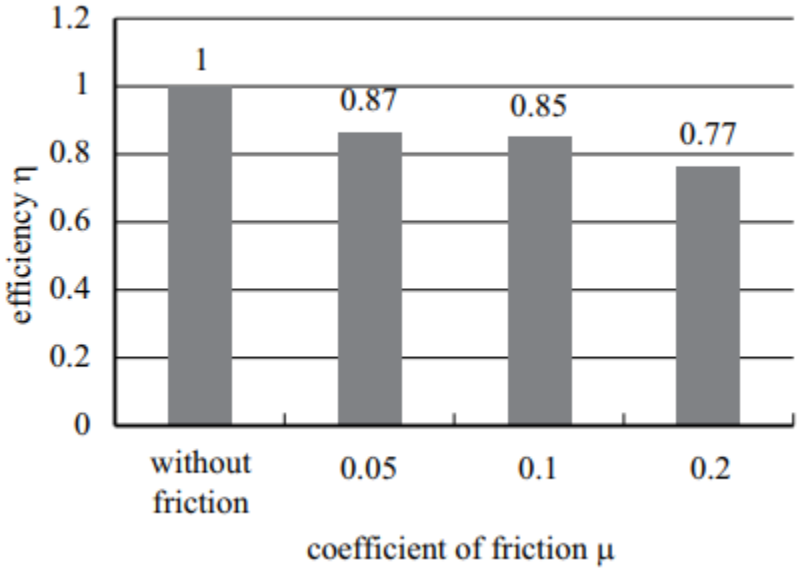

Fig. 39 ***Efficiency dependence on the friction coefficient*** *[32].*

If the values of the contact force with different friction values are analyzed is obvious that the one without friction has better efficiency and as the friction increases, the efficiency decreases. Thus, as a conclusion is very important to take into consideration the effect of friction and other variables too such as inertia and backlash because this can make a critical difference in the gearbox selection for a regenerative shock absorber or any other type of task.

3.3 Cycloid model

In this section a Cycloid Drive model is described. The design variables, objective functions for the optimization of the volume and its functioning, and the different part types of it.

3.3.1 Cycloid Drive

Cycloid speed reducers are mechanisms that are characterized by their disk shape form, wide opportunity of ratios depending on the task, a high efficiency in the transmission compared to other gear boxes in the literature, low noise functioning, and smooth and quick response. They can be implemented in all kinds of machines, [32] especially in robotics.

The Cycloid Drive optimization for the volume is very important because there are some restrictions related to space availability in the vehicle suspension and how a great volume can affect vehicle dynamics. To obtain the main task, 5 design variables were selected based on Wang's work and one objective function. For the optimization a Particle swarm optimization method is used.

3.3.1.1 Design Variables

The design variables are five:D_z, d_z, B , k_1, d_w. D_z is the pin gear diameter and its basically the diameter of the Cycloid drive itself, d_z is the diameter of each pin, B is the width for each of the cycloid gears, and d_w is the diameter of the cylindrical pin mounted in the output mechanism [32].

3.3.1.2 Objective function volume of Cycloid Drive.

The radial dimension of the Cycloid Drive is basically the diameter of the pin housing D_z [33]. The axle length is determined by the width the sum of the the cycloid gear B and the gap that exists between the cycloid gears. In the following equation the volume objective function is presented as:

$$f_1(X) = \frac{\pi}{4} \cdot (D_Z + d_z + 2\Delta_1)^2 \cdot (2B + \delta) \tag{14}$$

Δ_1 is the thickness of each pin sleeve and δ is the gap that exists between the two cycloid gears and δ is defined by:

$$\delta = b - B$$

b is the width of the turning arm bearing, where cycloids are mounted.

3.3.1.3 Constraints

Several constraints are presented to ensure the proper functionating of the cycloid drive.

1. **Short amplitude coefficient.**

   The decrease of the short amplitude coefficient means that the pin will experience a bending stress increase [33]. The optimal range for the short amplitude coefficient is presented as:

$$g_1(X) = 0.45 - K_1 \leq 0 \tag{15}$$

$$g_2(X) = K_1 - 0.8 \leq 0 \tag{16}$$

2. **Cycloid tooth profile.**

   Cycloid tooth profile needs to avoid undercut, from the division of diameter external of the pin sleeves mounted in the pins to a pin gear diameter. The diameter of the pin sleeve and the diameter of the pin gear ratio should be less than the minimum coefficient of the theoretical tooth profile [32]. The following equation is as:

$$g_3(X) = \frac{d_z' + 2\Delta_1}{D_z} - \alpha_{min} \leq 0 \tag{17}$$

   Where:

$$\alpha_{min} = \frac{(1 + K_1)^2}{(1 + K_1 + Z_g K_1)^2} \tag{18}$$

3. **Maximum diameter of the cylindrical pin hole.**

   Between two adjacent cylindrical pin holes, a thickness T is mandatory to secure the strength in the cycloid gears, and in general terms, $T = 0.03D_z$ [36]. As a consequence, the maximum diameter of the cylindrical pin hole has constraints presented as:

$$g_4(X) = 2T - D_w + d_{sk} + D_1 \leq 0 \tag{19}$$

$$g_5(X) = T - D_w sin\frac{\pi}{Z_w} + D_{sk} \leq 0 \tag{20}$$

Z_w is the number of cylindrical pins. D_w is the diameter of the cylindrical pin hole distributed circle, which is defined as :

$$D_w = \frac{d_{fc} + D_1}{2} \tag{21}$$

d_{fc} is the diameter of the root circle of one cycloid gear. D_1 is the diameter of the cycloid gear center hole for both disks, which is also the external diameter of the turning arm bearing where cycloids are mounted.

d_{sk} is the diameter of the cylindrical pin hole, defined as :

$$d_{sk} = d_w + 2e \tag{22}$$

d_w is the external diameter of a cylindrical pin sleeve.

4. Pin-diameter coefficient.

Pin gears interference need to be avoided and to make sure the strength of the pin gear ring the value of K_2 pin-diameter coefficient is desired to be in the range of 1.25–4 [34]. This constraint conditions are presented as:

$$g_6(X) = 1.25 - K_2 \leq 0 \tag{23}$$

$$g_7(X) = K_2 - 4 \leq 0 \tag{24}$$

Where:

$$K_2 = \frac{D_z}{d_z' + 2\Delta_1} \cdot \sin(\frac{\pi}{Z_B}) \tag{25}$$

5. Contact strength of the cycloid gear and the pin gear.

Fatigue scuffing and pitting failure at tooth surface needs to be avoided. The meshing between the cycloidal gear teeth and the pin teeth should meet the contact strength [32]. The Hertz theory is used for the contact stress (σ_H) between the pin gear and the cycloid gear. It is presented as:

$$\sigma_H = 0.418\sqrt{\frac{F_i E_d}{B\rho_d}} \tag{26}$$

E_d is the elastic modulus equivalent that exists between the pin gear and the cycloid gear, the meshing force F_i is applied at an specific position between the pin gear and the cycloid gear, and the contact point ρ_d is the equivalent curvature radius. This constraint is presented as follows:

$$g_8(X) = 0.418\sqrt{\frac{F_i E_d}{B\rho_d}} - \sigma_{HP} \leq 0 \tag{27}$$

6. Bending strength of the pin gear.

The failures of pins which result in a break is a very common failure typical for a cycloid reducer, therefore the maximal bending stress of the pin is mandatory that it needs to be minimized [34]. This constraint is presented as:

$$g_9(X) = \frac{44 \cdot L_1 \cdot L_2 \cdot T_v}{L \cdot K_1 \cdot Z_g \cdot D_z \cdot {d_z}'^3} - \sigma_{FP} \leq 0 \tag{28}$$

where σ_{FP} is the allowable bending stress.

and $L_1 = 0.5B + \delta' + 0.5\Delta$, $L_2 = 1.5B + \delta' + \delta + 0.5\Delta$, and $L = L_1 + L_2 = 2B + 2\delta' + \delta + \Delta$. D is the thickness of the external walls of the housing. δ' is the distance of the cycloid gear and the next body which is the internal face wall, and in general, $d'_z \leq \Delta \leq B$.

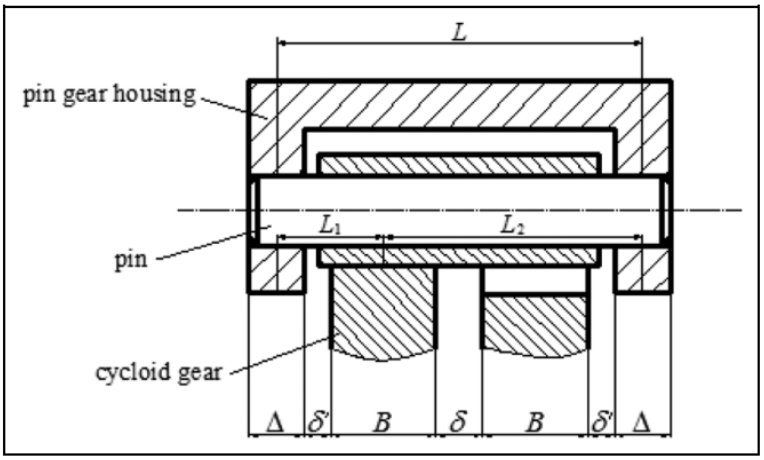

Fig. 40 ***Cycloidal transmission structure of pin gear with two pivots*** *[32].*

7. Contact strength between the cylindrical pin and the cylindrical pin hole.

The failure of the cylindrical pin and the cylindrical pin hole needs to be avoided [34]. Therefore, this constraint is presented as:

$$g_{10}(X) = 0.0949\sqrt{\frac{10 \cdot K_1 \cdot T_v \cdot D_z}{Z_w \cdot D_w \cdot B({r_w}^2 \cdot Z_b + \frac{D_z \cdot K_1}{2} r_w)}} - \sigma_{HP} \leq 0 \tag{29}$$

where r_w is the radius of the cylindrical pin sleeve, which can be defined as:

$$r_w = \frac{{d'}_w}{2} + \Delta_2 \tag{30}$$

where Δ_2 is the thickness of the cylindrical pin sleeve.

8. Bending strength of the cylindrical pin.

Bending strength constraint of the cylindrical pin mentioned by Rao [34],is shown as:

$$g_{11}(X) = \frac{96 \cdot T_v \cdot (1.5 \cdot B + \delta)}{Z_w \cdot D_w \cdot {d_w}'^3} - \sigma_{FP} \leq 0 \tag{31}$$

9. Life of the turning arm bearing

The turning arm bearing that is in the output mechanism and where the cycloid discs are mounted is as follows:

$$g_{12}(X) = L_h - \frac{10^6}{60n}\left(\frac{C}{F}\right)^{\frac{10}{3}} \leq 0 \tag{32}$$

L_h is the turning arm bearing life, n is the speed of the bearing rotation, C is the dynamic load and finally, F is the dynamical load.

$$F = 1.2R \tag{33}$$

Where R is the radial load on bearing

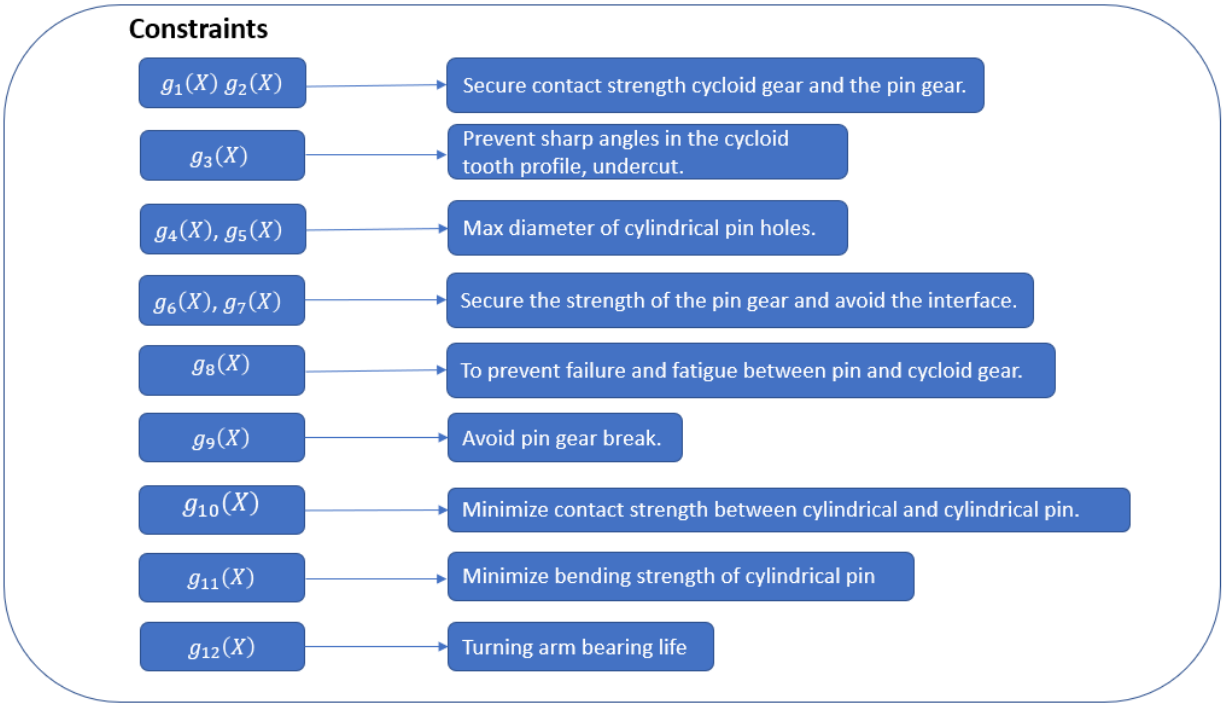

Fig. 41 **Cycloid drive constraints.**

3.3.1.4 Particle Swarm optimization

The concept of PSO basically is to create a swarm of particles that are moving in the search space looking for a goal or the place which best suits their needs given by a fitness function or objective function.

For this project to apply swarm optimization, the lower and upper boundaries and nonlinear constraints need to be set up for the algorithm to obtain the best volume for the cycloid transmission.

The boundaries are shown in table 7.

Table 7 **Upper and lower boundaries**

	$D_z(mm)$	$d_z(mm)$	$B(mm)$	k_1	$d_w(mm)$
LB	80	6	4	0.4	3
UB	120	12	17	0.8	55

With the boundaries and restrictions set up, initial values are required. The initial values need to be between the boundaries to run and then obtain the optimization volume value.

3.4 Electric Motor model

In this section is described the of electric motor model for the project that is attached to the cycloid transmission and the design parameters, Input parameters, Fixed design parameters, Material parameters, Derived parameters, and geometry.

3.4.1 Electric motor

For this work a permanent magnet DC motor is selected, where the constant motor flux is generated by the magnets. To fix some of the parameters and then determine the remaining as part of the design is what is proposed in this work. Fixing parameters is great when there is an idea about the overall motor volume allowed. The out put of this model is T_m which is the motor torque

3.4.1.1 Input parameters

The output of this model is the radial size of the electric motor that needs to be the same as the cycloid transmission to perfectly fit in position 1 of the suspension.
The input parameters are the length of the motor L which is crucial for this work, the stator outside radius R_{SO} that is basically the radius of the motor and the rotor outside radius R_{ro} .The stator outside radius, motor axial length, and rotor outside radius specify the overall motor size.

3.4.1.2 Design parameters

The parameters listed below are grouped according to function.
J_w which is the wire current density, it is the amount of charge per unit time that flows through a unit area of a chosen cross section, N_m is the number of magnet poles and N_s the number of slots. N_{ph} are the number of phases**,** generally is very uncommon to find a motor with more than three phases, g is the air gap is the air space between the rotor and stator of a motor.K_{st} is the lamination stacking factor. K_{cp} is the coil packing factor. α_m is the magnet fraction. ω_s is the slot opening measured in meters. $\omega_{sd}$is the shoe depth fraction and P_c is the operating point of a permanent magnet in a magnetic circuit.

Table 8 **Design parameters**

	Design parameters
J_w	Wire current density
N_m	The number of magnet poles
N_s	The number of slots
N_{ph}	The number of phases
g	Air gap
K_{st}	Lamination stacking factor
K_{cp}	Coil packing factor
α_m	Magnet fraction
ω_s	Slot opening

ω_{sd}	Shoe depth fraction
P_c	Operating point of a permanent magnet

3.4.1.3 Material parameters

B_R is the magnet remanence which depends on the material, μ_R is the magnet relative permeability which is the measure of magnetization that a material obtains in response to an applied magnetic field. μ_0 is the permeability of free space or vacuum permeability. It is derived from production of a magnetic field by an electric current or by a moving electric charge and in all other formulas for magnetic-field production in a vacuum.B_{max} material saturation that for this work would be iron.

Table 9 ***Material parameters***

	Material parameters
B_R	Magnet remanence
μ_R	Magnet relative permeability
μ_0	Permeability of free space
B_{max}	Material saturation

3.4.1.4 Derived parameters

Following design and material parameters, the derived parameters can be determined.

- The number of slots per magnet pole is defined as:

$$N_{sm} = \frac{N_s}{N_m} \tag{34}$$

  Where N_s is the number of slots and N_m is the number of magnet poles.

- The primary constraint on stator design is that the total number of stator slots be some even integer multiple of the number of phases:

$$N_s = N_{sp} N_{ph} \tag{35}$$

Where N_{sp} is the even integer number of slots per phase and N_{ph} is the number of phases.

- The number of slot per pole is determined as:

$$N_{spp} = \frac{N_s}{N_m N_{ph}} = \frac{N_{sp}}{N_m} \tag{36}$$

- θ_p is the angular pole pitch in mechanical radians:

$$\theta_p = \frac{2\pi}{N_m} \tag{37}$$

- The slot pitch in electrical radians is:

  θ_s is the angular slot pitch in mechanical radians:

$$\theta_s = \frac{2\pi}{N_s} \tag{38}$$

- k_p is the ratio of the peak flux linked :

$$k_p = \frac{int(N_{spp})}{N_{spp}} \tag{39}$$

- The stator inside radius is defined as:

$$R_{si} = R_{sb} - d_s = R_{ro} + g \tag{40}$$

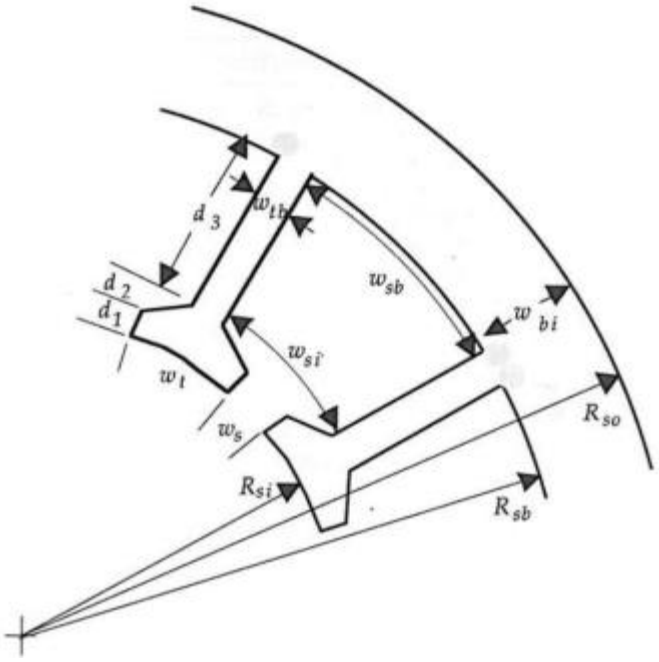

Fig. 42 **Slot geometry** [39]**.**

- The pole pitch at the inside surface of the stator is related to the angular pole pitch by:

$$\tau_p = R_{si} \cdot \theta_p \tag{41}$$

- The slot pitch at the rotor inside radius is:

$$\tau_s = R_{si}\theta_s \tag{42}$$

- The tooth width at the stator surface is calculated as:

$$\omega_t = \tau_s - \omega_s \tag{43}$$

- And the distribution factor is determined:

(44)

$$k_d = \frac{sin(N_{spp}\frac{\theta_{se}}{2})}{N_{spp}\sin(\frac{\theta_{se}}{2})}$$

3.4.1.5 Geometry

Now that some parameters are set, we can determine the remaining of the model design for the geometry.

- In terms of permeance coefficient the concentration factor is:

$$C_{\emptyset} = \frac{A_m}{A_g} = \frac{2\alpha_m}{1+\alpha_m} \quad (45)$$

- A longer relative magnet length increases the available air gap flux density, so the operating point pf the magnet is found with the permeance coefficient:

$$l_m = P_c \cdot (g \cdot C_{\emptyset})$$

$$\theta_{se} = \frac{\pi}{N_{sm}} \quad (46)$$

- A motor with lower magnet leakage flux gives higher performance, the closer is to 1 the leakage factor is the better.

$$k_{ml} = 1 + \frac{4l_m}{\pi\mu_R\alpha_m} l_n\left[1 + \pi\frac{g}{(1-\alpha_m)\tau_p}\right] \quad (47)$$

- When the slots are directly opposite each other the approximation is with the carter coefficient:

$$k_c = \left[1 - \frac{1}{\frac{\tau_p}{\omega_s}(5\frac{g}{\omega_s}+1)}\right]^{-1} \quad (48)$$

- The air gap mean cross section is:

$$A_g = \tau_p L \frac{(1+\alpha_m)}{2} \tag{49}$$

- In terms of magnet and air gap flux densities, this expression becomes:

$$B_g = \frac{C_\emptyset}{1 + \frac{\mu_R k_c k_{ml}}{P_c}} \tag{50}$$

- This flux density represents the average value crossing the air gap. When the stator is slotted, the actual flux density over the slots will be lower because of the longer flux path there.

  Where air gap flux is determined as:

$$\emptyset_g = B_g \cdot A_g \tag{51}$$

- The flux density allowed in the back iron is B_{max} , so the back iron width is:

$$\omega_{bi} = \frac{\emptyset_g}{2B_{max} k_{sb} L} \tag{52}$$

  where k_{sb} is the lamination stacking factor.

- If the flux density allowed in the teeth is also B_{max} , the required tooth width is:

$$\omega_{tb} = \frac{\emptyset_g}{N_{sm} B_{max} k_{sb} L} = \frac{2}{N_{sm}} \omega_{bi} \tag{53}$$

- The stator base radius R_{sb} and rotor inside radius R_{ri} is determined as:

(54)

$$R_{sb} = R_{so} - \omega_{bi}$$

(55)

$$R_{ri} = R_{ro} - l_m - \omega_{bi}$$

- The width of the slot bottom is given by:

$$\omega_{sb} = R_{sb}\theta_s - \omega_{tb} \quad (56)$$

- The slot width just beyond the shoes is:

$$\omega_{si} = (R_{si} + \alpha_{sd}\omega_{tb})\theta_s - \omega_{tb} \quad (57)$$

- The slot fraction is defined as:

$$\alpha_s = \frac{\omega_{si}}{\omega_{si} + \omega_{tb}} \quad (58)$$

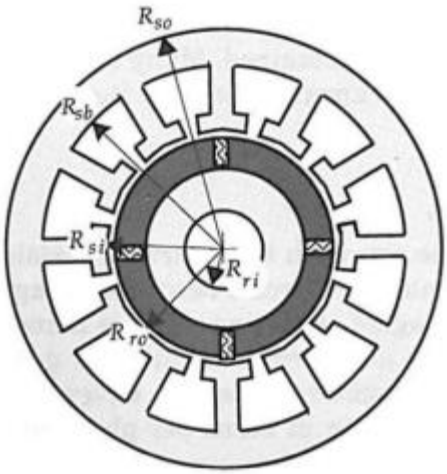

Fig. 43 **Radial flux motor topology** [39].

- Knowing the back iron widths of the rotor and stator ω_{bi} and the tooth width ω_{tb}. With this dimension all other dimensions can be found, so the particular slot depth is:

$$d_s = R_{sb} - R_{ro} - g \tag{59}$$

- The conductor slot depth is:

$$d_3 = d_s - \alpha_{sd}\omega_{tb} \tag{60}$$

- Given that $d_s = d_1 + d_2$+d_3 and

$$d_1 + d_2 = \alpha_{sd}\omega_{tb} \tag{61}$$

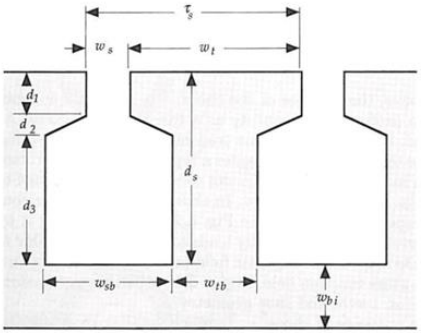

Fig. 44 **Slot geometry** [39].

- The slot cross-sectional area available for conductors is:

$$A_s = d_3\left[\theta_s\left(R_{sb} - \frac{d_3}{2}\right) - \omega_{tb}\right] \tag{62}$$

It is assumed that no matter what winding approach is used, all coils making up a phase winding are connected in series. This assumption maximizes the back emf and minimizes the current required per phase to produce the required rated torque [40].

if the magnets are skewed, the skew factor must be included. Inclusion of these terms gives a final torque for a three-phase expression of:

$$T_m = \frac{3}{2} N_m k_d k_p k_s B_g L R_{ro} N_{spp} n_s i \tag{63}$$

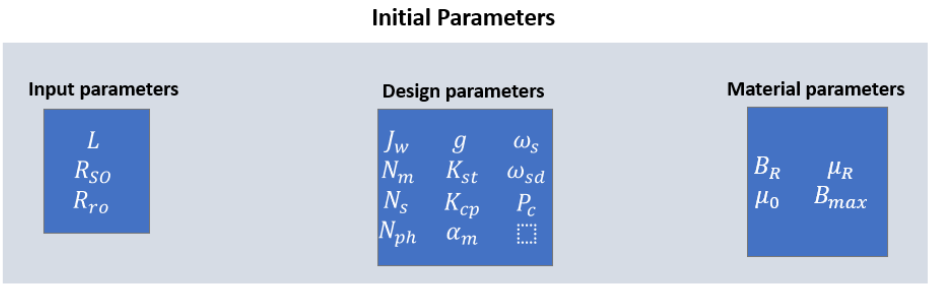

Fig 19. Initial parameters [12].

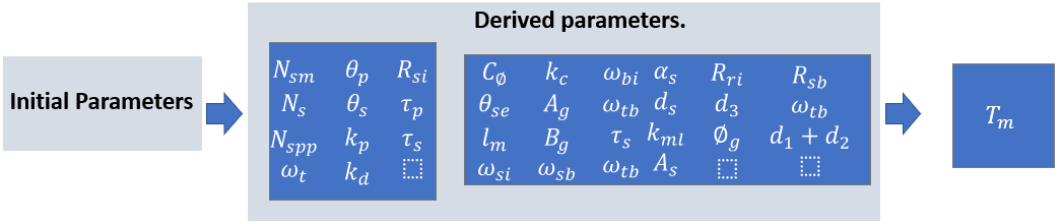

Fig. 45 ***Electric Motor model diagram***

With all these equations the maximum torque for the Electric Motor is obtained. This output is very important to then make and optimization with both the motor and Cycloid Drive models.

3.5 Optimization strategy

Now that the models for the Cycloid drive and electric motor were presented, can be said that these two models involve many variables. To connect these two models and find the optimal solution for this project, a multi variable optimization is required. First the cycloid

optimization is described, next how it connects with the electric motor model and finally the final optimization process.

3.5.1 Multi variable optimization.

The Cycloid Drive optimization model has 5 design variables: D_z, d_z, B , k_1, d_w, and as objective function the volume of the Cycloid. Once the best volume is obtained, the D_z value which is the diameter of the pin gear distributed circle is used as input for the electric motor model where the stator outside radius R_{SO} is basically the radius of the electric motor as:

$$\frac{D_z}{2} = R_{SO} \tag{64}$$

Then, in the electric motor model K which is the Torque per unit length is equivalent to all the variables from eq 64 except for L (length of the electric) motor as shown:

$$K = \frac{3}{2} N_m k_d k_p k_s B_g R_{ro} N_{spp} n_s i \tag{65}$$

Next, two equations are presented to obtain motor torque T_m , the first one determined with the Torque of gearbox T_g times gearbox ratio τ_g from eq 13 and T_m from the electric motor model of eq 64:

$$T_m = T_g \cdot \tau_g \tag{66}$$

$$T_m = K * L \tag{67}$$

Now these two equations are matched and solve for L which is the length of the electric motor as shown:

$$L = \frac{T_g * \tau_g}{K} \tag{68}$$

Then K is Maximized to get the best value of R_{ro}.Thus, with the obtained values of L and R_{SO} the volume of the motor V_m is calculated plus the volume of the cycloid drive V_c of eq 15.

$$V_m = \pi \cdot L \cdot {R_{SO}}^2 \tag{69}$$

And the total volume is:

$$V_T = V_m + V_c \tag{70}$$

This total volume represents the volume of the cycloid drive and the electric motor coupled.

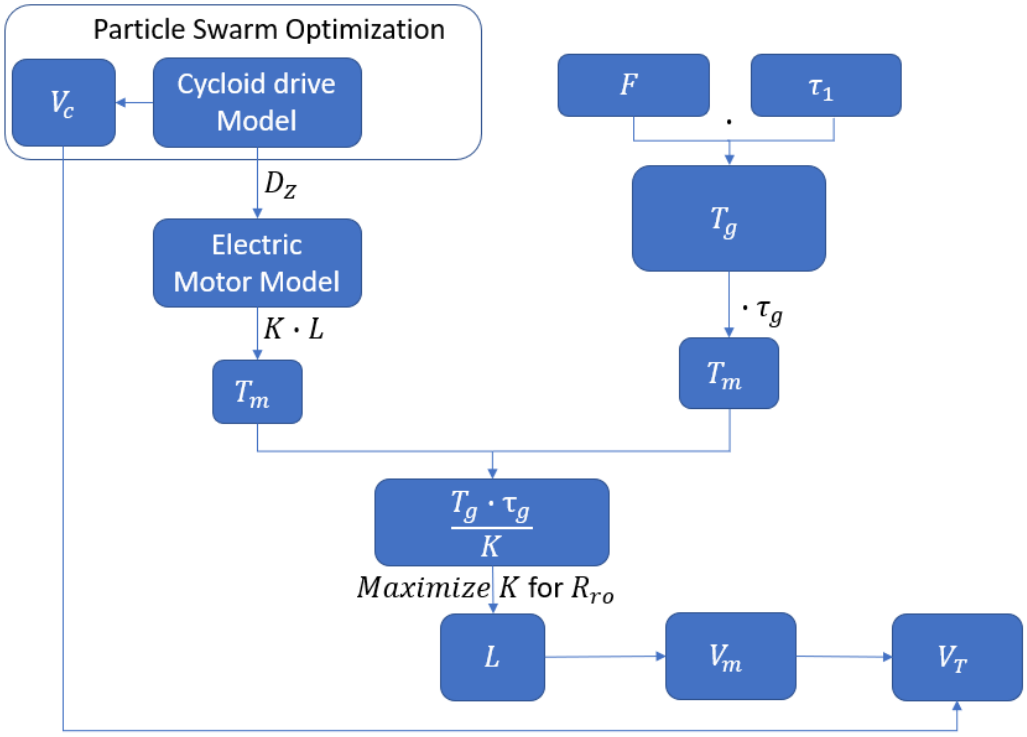

Fig. 46 **Diagram of the optimization strategy.**

3.6 Optimization Output

The results for the optimization are presented while the Tooth number of the Cycloid gear is increasing. The final dimension for both elements together is important to make sure if the mechanism fits in the EV-TEC suspension space.

3.6.1 Multi variable optimization

A multivariable optimization is a very complex task because it involves many variables and constraints that need to be satisfied to get the final target. The Optimization for the cycloid transmission is very important because the first design variable D_Z is fundamental to connect the cycloid transmission with the electric motor.

The optimized values for the cycloid transmission are presented in table 10

Table 10 **Cycloid transmission optimized values**

Cycloid Drive								
			Design variables					**Objective**
Tooth number of the cycloid gear	Tooth number of the pin gears	Length of Cycloid T.	Diameter of pin gear distributed circle	Diameter of pin	Width of cycloid gear	Short width coefficient	Cylindrical pin	Volume
Z_g	Z_b	$L(mm)$	$D_z\,(mm)$	$d_z\,(mm)$	$B(mm)$	k_1	$d_w\,(mm)$	$f_1(m^3)$
11	12	32.1	116.7	6.2	4.1	0.64	10.3	1.82e-04
12	13	32	104.8	6.0	4.0	0.8	4.8	1.49e-04
13	14	32	97.8	6.0	4.0	0.8	3.5	1.32e-04
14	15	32	93.8	6.0	4.0	0.73	3.6	1.23e-04
15	16	32	89.5	6.0	4.0	0.71	3.0	1.13e-04

- Notice that table 10 ends when the tooth number of cycloid gear is 15 and pin gear is 16, this occurs because the Electric Motor angular speed was limited to 15000 rpm and to obtain it as seen in eq 11, the gearbox ratio is needed. Thus, as the cycloid gear number increase, the angular speed also increases.
- Can be observed that D_z is the variable that affects the most in the volume of the Cycloid drive
- The Length of the Cycloid Drive varies according to B and many other parameters as seen in Fig.35, but because these parameters are fixed the width of the cycloid gears have a great impact in the axial length.
- The last row are the optimal results for the number of teeth, design variables and objective Volume

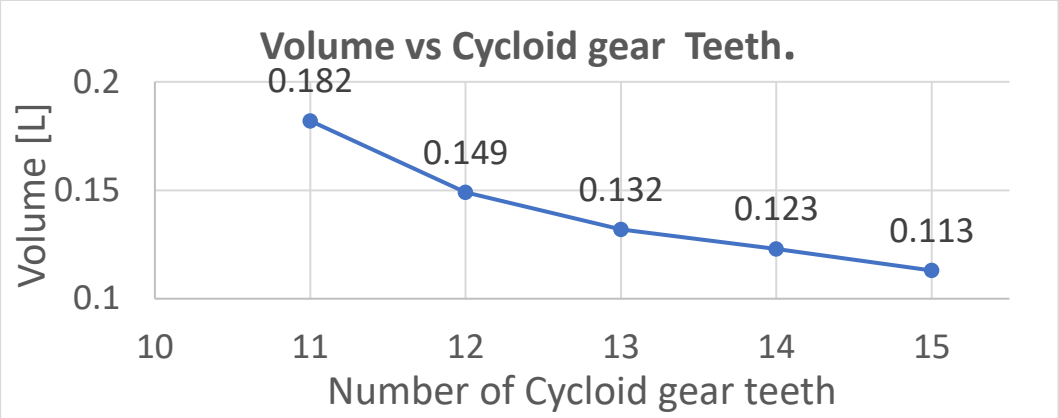

Fig. 47 **Cycloid gear teeth and volume Cycloid gear teeth and volume**

For the Electric Motor the optimal values are presented in table 11.

Table 11 **Electric Motor values**

Input parameters				
Axial Length	Stator outside radius	Rotor outside radius	$Volume$	$Torque$
$L(mm)$	$R_{so}\ (mm)$	$R_{ro}\ (mm)$	$V_m(m^3)$	$T_m(Nm)$
263	63.7	26.1	3.34e-04	5.82
298	57	23.2	3.08e-04	4.81
327	53.7	21.7	2.82e-04	4.045
34.2	48.9	19.6	2.57e-04	3.44
33.9	47.17	18.8	2.32e-04	2.97
33.4	44.85	17.8	2.10e-04	2.27

- It is important to notice that the values for R_{so} are half of D_z from table 11 which means that both components will have the same diameter when working together.
- Notice that when the motor reaches a very small diameter the axial length is increased dramatically. For this project is mandatory to avoid very large components because that may cause interference with other components in the suspension. Is preferred a radial size increase instead.
- When the Axial Length decreases the radius increases with this a disk-shaped form is achieved which is something desired for this work according to the state of the art.
- Notice that as T_m decreases the V_m also decreases, because there is almost a linear relation between them [36].
- The last row are the optimal results for the Axial Length, Stator, Rotor radius, volume, and Electric Motor Torque.

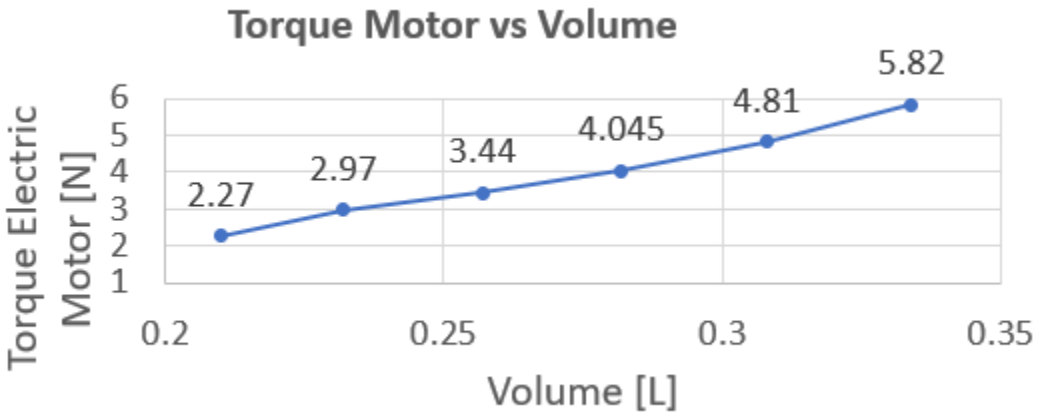

Fig. 48 **Motor Volume and Torque**

Table 12 **Regenerative system final dimensions**

	$\boldsymbol{Diameter(mm)}$	$\boldsymbol{Axial\ length(mm)}$	$\boldsymbol{Volume(m^3)}$
Cycloid Transmission	89.5	32	1.13e-04
Electric motor	89.5	33.5	2.10e-04
Total		65.5	3.23e-04

Now, with the final dimensions, the total length of the components when working together are shown as well as the total volume in table 12.

3.7 Electric Motor Torque calculation with FEM

The T_m was also obtained with Finite Element Method Magnetics software Femm. The results are similar to the obtained with the analytical model.

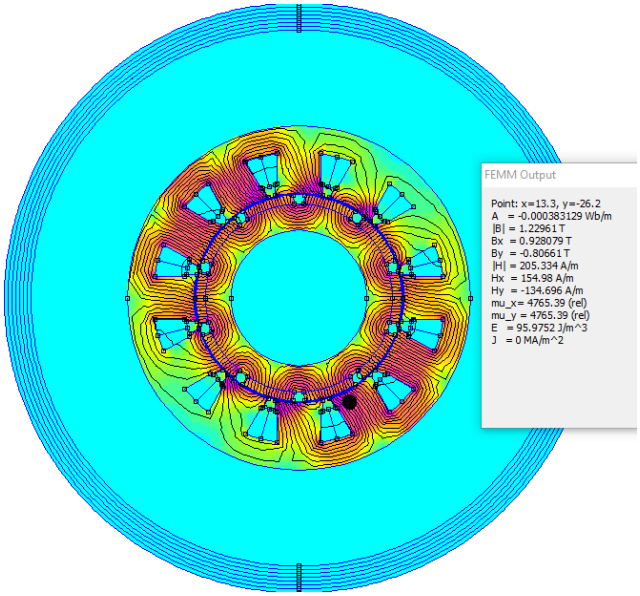

Fig. 49 ***Electric Motor Torque using FEM***

- A 2D model of the Electric Motor was created with 10 magnets and 12 slots. After labeling every part of the 2d model, and setting the phases order, the model is divided in two groups.
- Next, the meshing is performed, automatically generated by femm.
- When looking at the density plot in Fig 42. Can be appreciated that in the black dot there is a magnet remanence of 1.22 T which is the most saturated part of the electric motor because there is a magnet in front of it. In the analytical model the remanence is 1.25 T
- The T_m is calculated with the numerical FEM and it has a value of 2.48 Nm.
- The T_m with the analytical model is 2.27 Nm.

$$\frac{2.27}{2.48} = 0.9153$$

Which means that according to the numerical FEM the T_m has a 10% more torque value than the analytical model.

3.8 Vertical dynamics and design

To be sure that the electric motor is capable of handling the demand of the actuator for the different type of strategies, its important to analyze the different type of scenarios.

The first scenario, is when the Electric Motor is not capable of handling the Skyhook RMS force , which can produce an increase in stress and heat, leading to a failure in the Electric Motor.

The second scenario is when the Electric Motor is able to deal with the force of the most demanding energy configuration which is Skyhook and therefore the design of the motor is suitable or the task.

To answer this problematic, is necessary to mention that a possible solution for scenario 1 is to make the motor larger to the point where it can handle with no further problems the actuation necessities. Also, it's important to state that the design or the Electric Motor was with the worst case, which means a maximum force for the suspension of 2000N and current density of 20 A/mm^2 where the electric motor can deliver torque for around 10 seconds and then it stops. The RMS force of the Skyhook configuration is 215 N at 35 km/h in type C road profile.

Because the point o comparison is in the same point a simple rule of three can solve the problematic.

$$\frac{2000\ N \cdot 6\ \ A/mm^2}{20\ \ A/mm^2} = 600\ \text{N}$$

The force of the Electric Motor with 6 A/mm^2 is 600 N and the demand o the skyhook actuator is 215 N of force at A/mm^2, which means the Electric motor design can handle the demands for the Skyhook force. Thus, the motor design falls in the scenario 2.

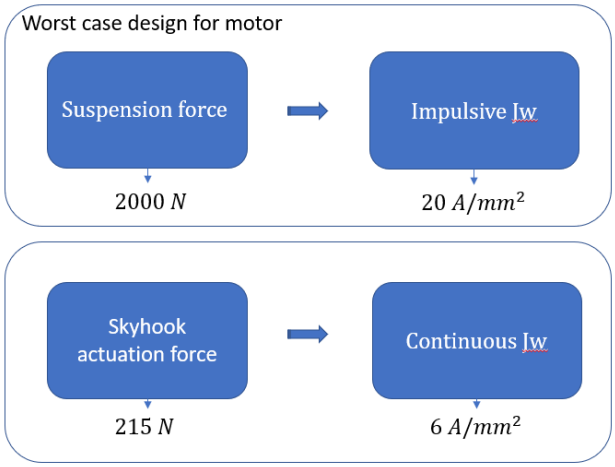

Fig. 50 ***Diagram of suspension force and Skyhook force.***

3.9 Target suspension & linear-to-rotary ratio

Once the cycloid transmission is selected, the final position of the transmission and electric motor needs to be determined. To determine the position, first the suspension type need to be explored to see if there is space to place the entire mechanism without interfering with the elements that belong to the suspension. The EV-TEC has a double wishbone suspension that belongs to a 2008 Yamaha rhino utilitarian vehicle [25]. The suspension contains the parts shown on Fig 40.

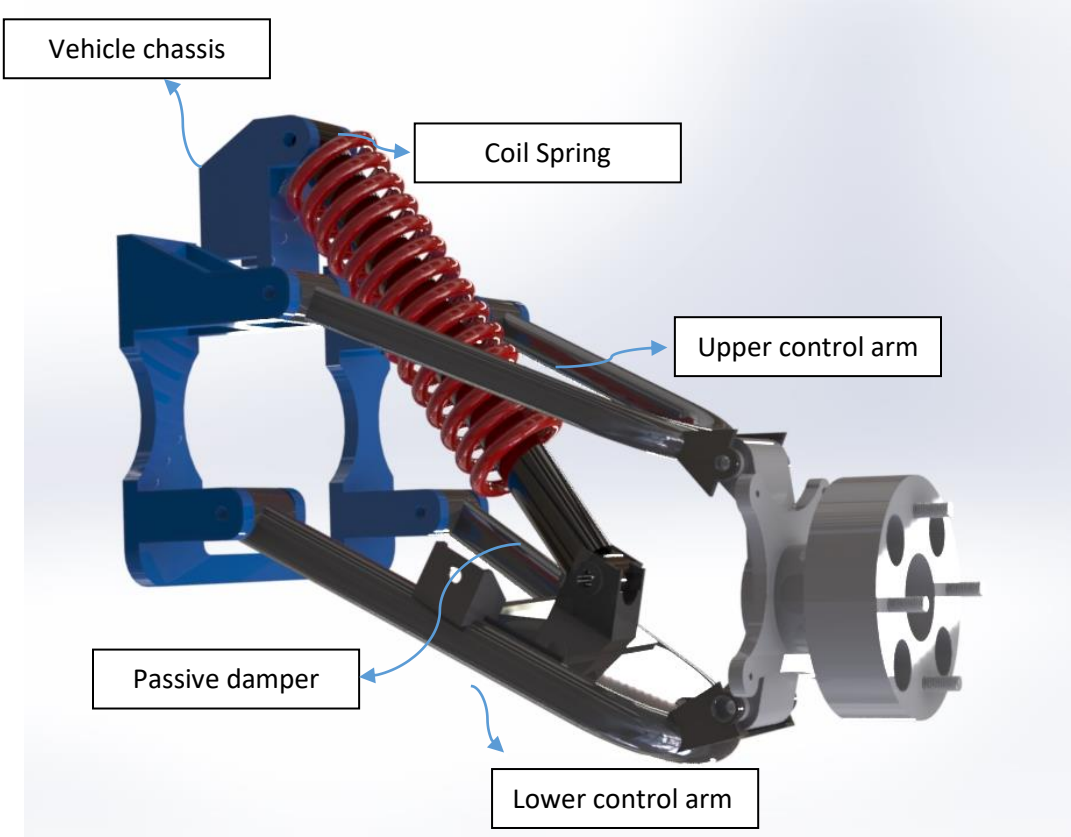

Fig. 51 **Ev-Tec Double wishbone suspension** [26]

Since this EV tec vehicle has plenty of space in the rear suspension as seen on Fig.41 the mechanisms can be positioned in both corners in the upper or control arm.

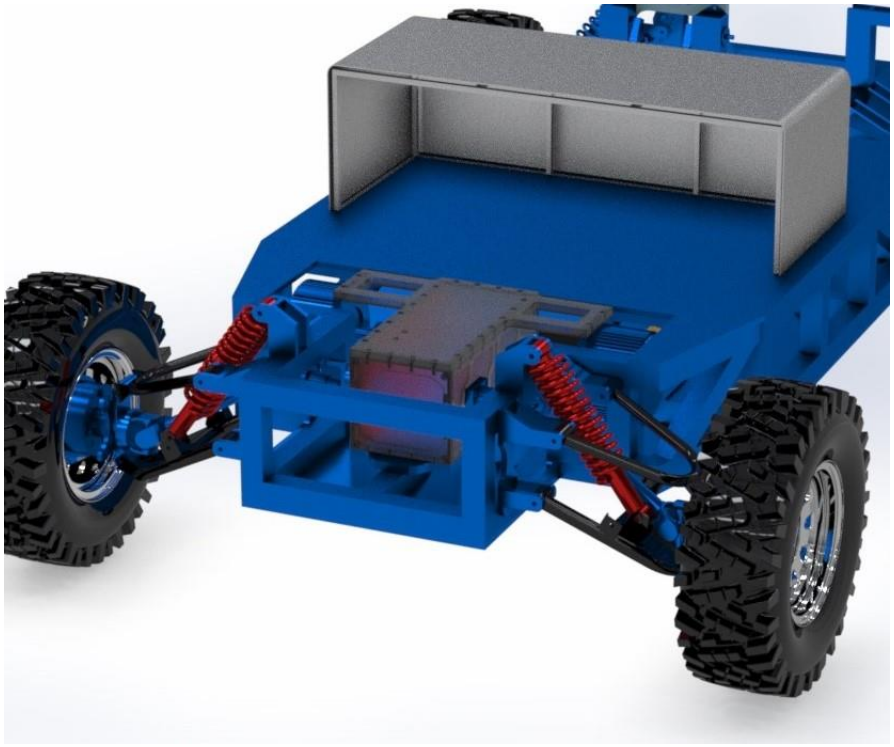

Fig. 52 **Ev-Tec rear double wishbone suspension** [26].

To determine the position of the mechanisms, there are some points to consider.

- No interference with other parts of the suspension is mandatory
- Easy to mount
- The Suspension transmission ratio needs to be lower

There are two possible options for the device where there is no interference with other elements of the suspension, these positions are shown in Fig 42. Also, it's important to notice that these two positions have an easy access, but to determine the final position the suspension transmission ratio needs to be obtained for the two options.

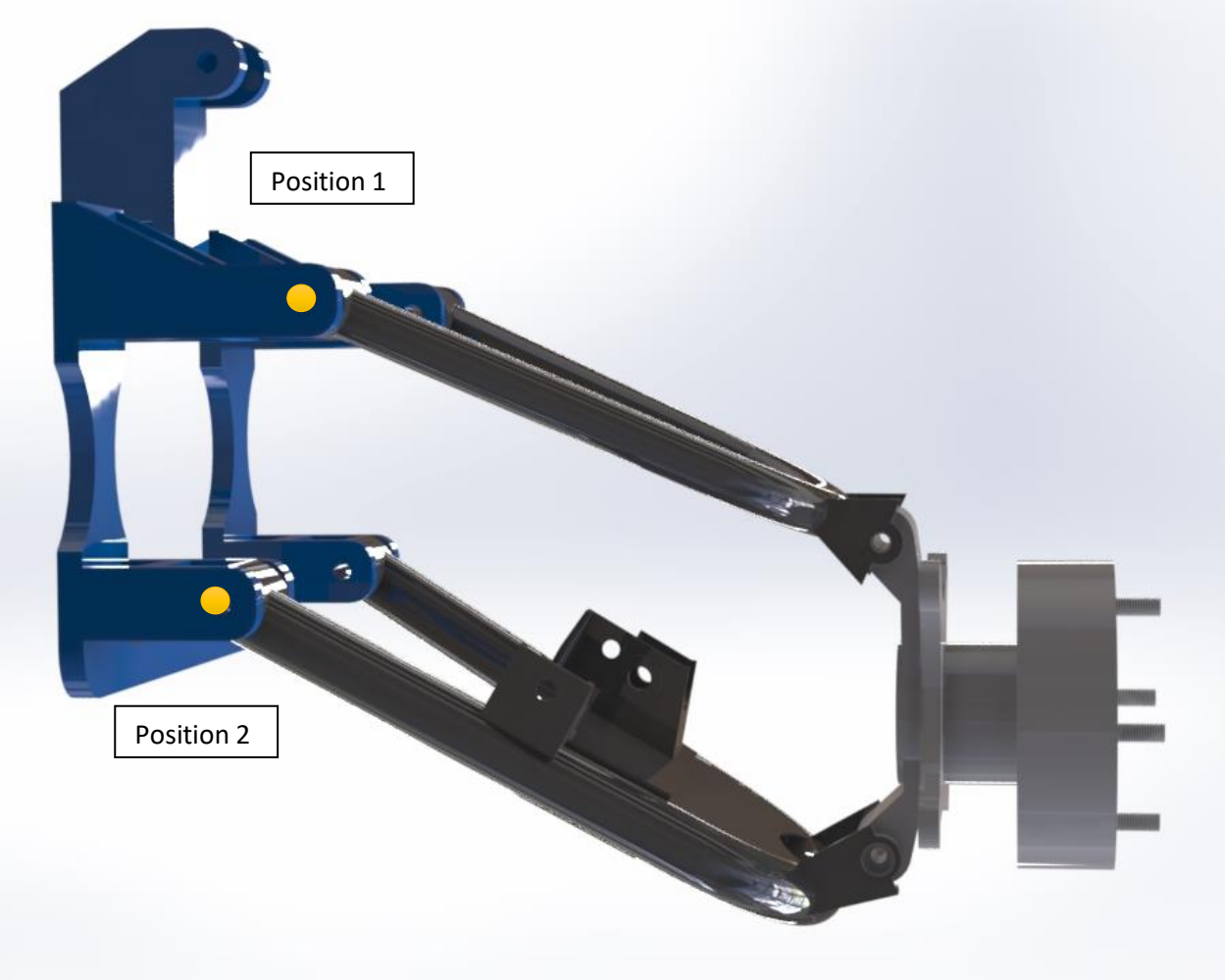

Fig. 53 **Possible locations spotted in yellow for the energy recovery mechanism** [25].

The suspension transmission ratio consists of the angular displacement measured at the points where the suspension control arms are attached to the frame versus the vertical wheel displacement.

The results are:

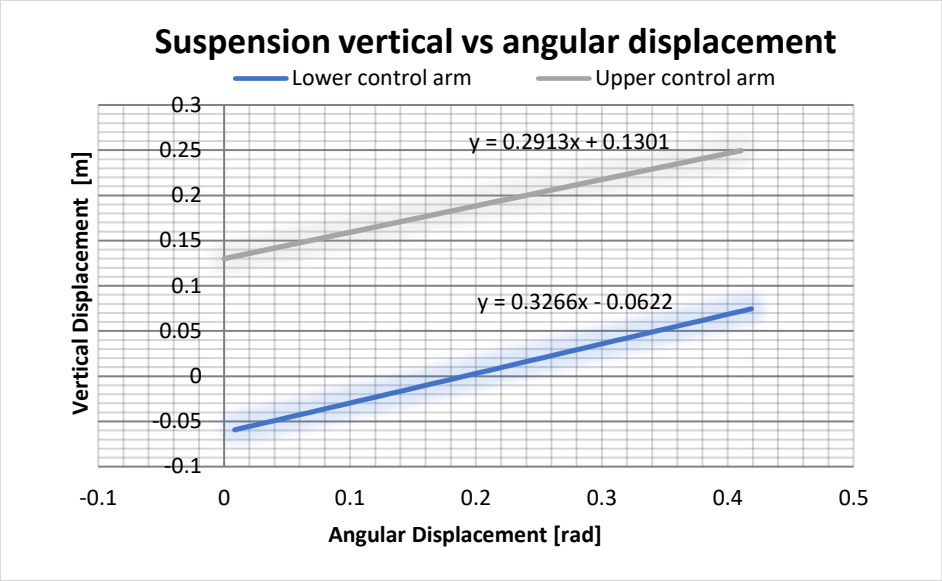

Fig. 54 **Vertical displacement vs angular displacement.**

- The transmission ratio of the two possible options is shown on Fig. 43. Can be appreciated that the upper control arm has lower value of 0.2913 $\frac{m}{rad}$ versus the value of the lower control arm of 0.3266 $\frac{m}{rad}$.

To determine which value suites better for this work we need set a series of steps to determine the best configuration.

- First, the vertical force approximation for the suspension to make the calculations is $F = 2000[N]$. This vertical force times transmission ratio is the input torque for the transmission. This input torque at the transmission don't need to be high because otherwise, it will require a great conversion from high torque to high speed and low torque which means and increase in diameter d of the transmission as seen on conclusions in the previous section on Table 6.
  For the position 1:
  Vertical Force from suspension= 2000[N]

$$2000[N] \cdot 0.2913 \frac{m}{rad} = 583\ [Nm]$$

To obtain an output torque that is around the desired values for the electric motor a reduction near to 225$[N]$ is required. To obtain this, 2 stages for the cycloid are needed. Each stage is $\frac{1}{15}$ in reduction ratio and because there are two:

$$\tau_g = \frac{Z_b - Z_g}{Z_g} \tag{71}$$

$$\tau_g = \frac{1}{15}$$

$$(\frac{1}{15})^2 = \frac{1}{225}$$

So, by dividing 583$[Nm]$ over 225$[Nm]$ the result is:

$$Output\ Torque\ motor = \frac{583[Nm]}{225\ [Nm]} = 2.59\ [Nm]$$

- For position 2:
  Vertical Force from suspension= 2000[N]

$$2000[N] \cdot 0.3266 \frac{m}{rad} = 653\ [Nm]$$

To obtain an output torque that is around the desired values for the electric motor a reduction near to 200$[N]$ is required. To obtain this, 2 stages for the cycloid are needed. Each stage is $\frac{1}{15}$ in reduction ratio and because there are two:

$$(\frac{1}{15})^2 = \frac{1}{225}$$

So, by dividing 583$[Nm]$ over 225 $[Nm]$ the result is:

$$Output\ Torque\ motor = \frac{653[Nm]}{225\ [Nm]} = 2.9\ [Nm]$$

In conclusion the upper control arm position 1 is selected to mount the mechanisms. Because the output torque is lower in that position and as seen in table 7 and Fig 34. The greater the torque, the bigger the transmission and therefore its mass increases and it affects the dynamics of the vehicle, so by selecting the lower output torque, a smaller mechanism is obtained.

4. Validation and Cycloid regenerative shock absorber

In this chapter the validation with the parameters obtained in the previous chapter are presented and the cycloid drive and the electric motor are shown individually, coupled together, and mounted in position 1 in the EV-TEC.

4.1 Validation

The obtained results in the optimization of the previous chapter are tested with Simscape for both the Skyhook and Groundhook configuration.

4.1.1 Skyhook validation

The Skyhook configuration is presented with the Cycloid drive regenerative shock absorber.

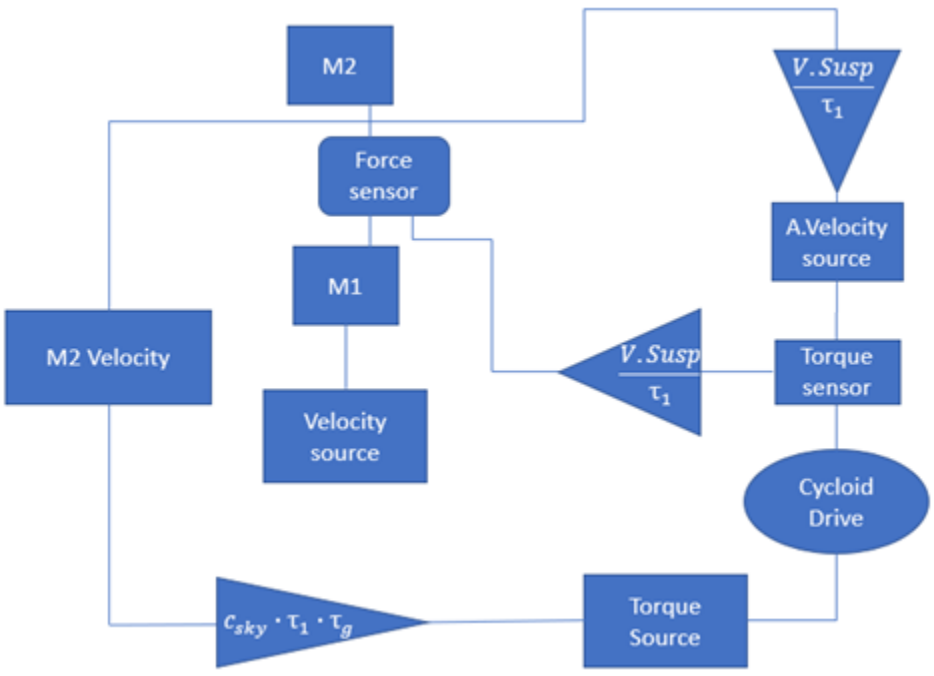

Fig. 55 **Skyhook validation.**

The velocity source receives a signal from the white noise through a gain that goes into the unsprung mass 1. Between the mass 1 and 2 there is a force source that represents the actuator.

The actuator gets a signal of force that comes from the cycloid drive which receives angular velocity from one side and torque from the other one. Notice that the velocity comes from mass 2 for the Skyhook configuration.

4.1.2 Groundhook validation

The Groundhook configuration is presented with the Cycloid drive regenerative shock absorber.

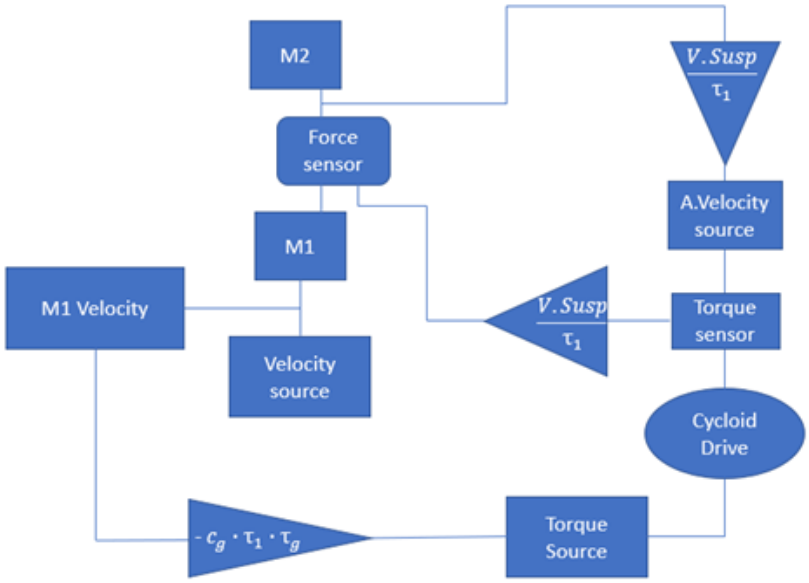

Fig. 56 **Groundhook validation.**

The velocity source receives a signal from the white noise through a gain that goes into the unsprung mass 1. Between the mass 1 and 2 there is a force source that represents the actuator. The actuator gets a signal of force that comes from the cycloid drive which receives angular velocity from one side and torque from the other one. Notice that the velocity comes from mass 2 for the Groundhook configuration.

4.1.3 Validation results and comparison

The results of the validation with the Cycloid regenerative shock absorber are displayed for the performance indexes, road handling and weighted acceleration compared to the values obtained in table 4.

Table 13 **Comparison table**

	Skyhook configuration		**Groundhook configuration**	
	Theoretical	Validation	Theoretical	Validation
Road handling	0.61	0.79	0.34	0.26
Weighted acceleration[$\frac{m}{s^2}$]	0.3	0.33	2.46	2.6

Can be concluded that the results from the Skyhook and Groundhook configurations do not vary much, there is a slightly difference with the validation getting higher values. At this point can be concluded that is feasible for the cycloid regenerative shock absorber to replace a regular shock absorber.

4.2 Cycloid drive

With the final dimensions obtained in the previous chapter, 3D models were created using Solid Works for the cycloid drive.

Table 14 **Cycloid Drive final values**

Cycloid Drive							
			Design variables				
Tooth number of the cycloid gear	Tooth number of the pin gears	Length of Cycloid T.	Diameter of pin gear distributed circle	Diameter of pin	Width of cycloid gear	Short width coefficient	Cylindrical pin
Z_g	Z_b	$L(mm)$	$D_z\,(mm)$	$d_z\,(mm)$	$B(mm)$	k_1	$d_w\,(mm)$
15	16	32	89.5	6.0	4.0	0.71	3.0

4.2.1 Input Mechanism and cylindrical pin

The input mechanism final 3D modeling is as shown in Fig 48.

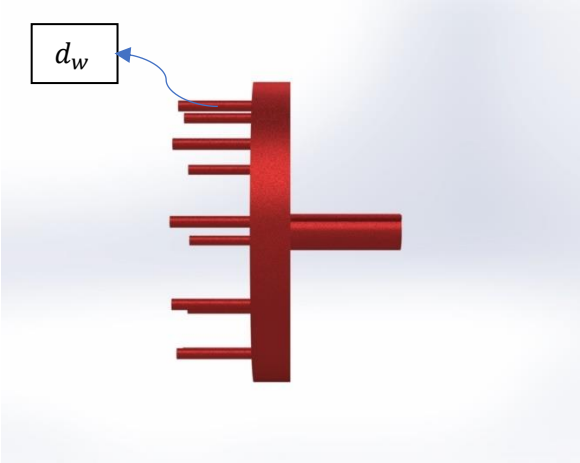

Fig. 57 ***Input mechanism***

The input mechanism:

- Is connected in the control arm bush of the suspension rotating along the upper control arm of the suspension.
- Rotates slowly, but with great torque
- Was connected ideally.

4.2.2 Cycloid gears

The cycloid gears 3D model is as shown in Fig 49.

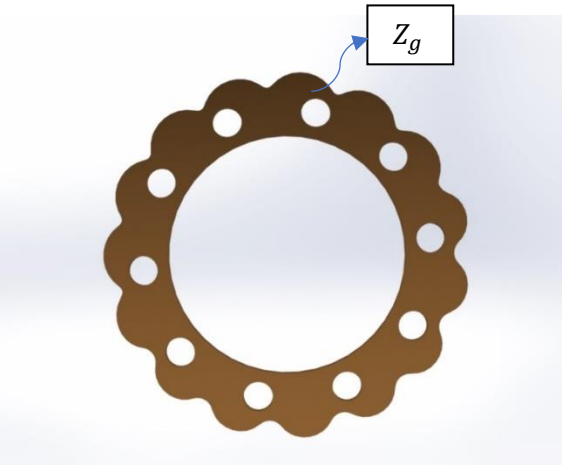

Fig. 58 ***Cycloid gear***

The Cycloid gears:

- Are mounted in the output mechanism.
- Rotate by the cylindrical pins.
- Have a high speed rotation.

4.2.3 Pin gear

The pin gear 3D model is as shown in in Fig 50.

Fig. 59 ***Pin gear***

The pin gear:

- Is where the pins are located
- Contains the Cycloid gears
- Remains fixed

4.2.4 Output mechanism

The pin gear 3D model is as shown in in Fig 51.

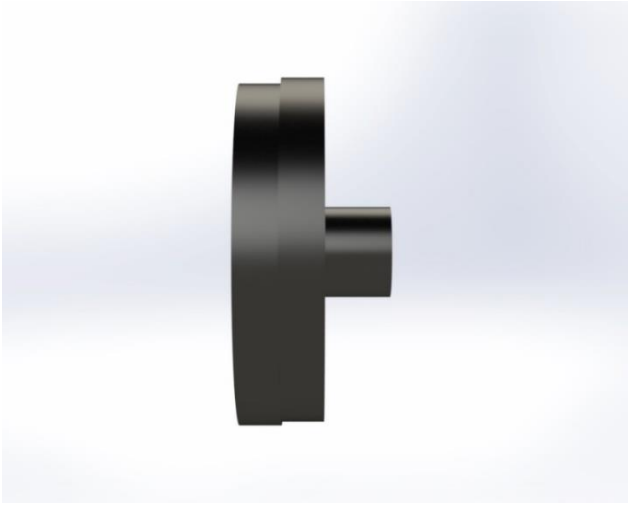

Fig. 60 ***Output Mechanism***

The Output mechanism:

- Is where Cycloid gears are mounted.
- Spins fast, but with lower torque

4.3 Electric Motor

With the final dimensions obtained in the previous chapter, all the 3D models were created using Solid Works for the Electric Motor.

Table 15 **Electric Motor final values**

Input parameters		
Axial Length	Stator outside radius	Rotor outside radius
$L(mm)$	$R_{so}\ (mm)$	$R_{ro}\ (mm)$
33.4	44.85	17.8

4.3.1 Stator

The Stator 3D model is as shown in in Fig 52.

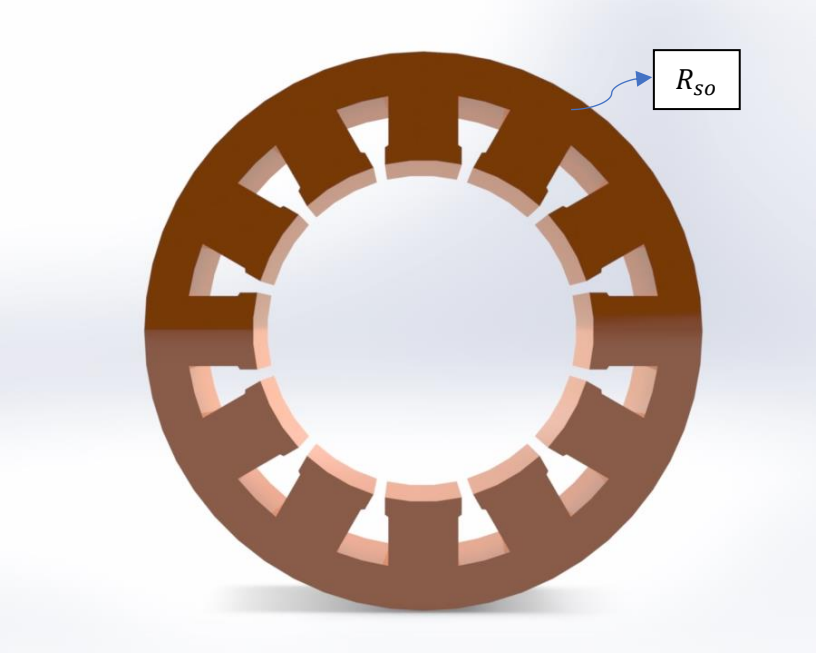

Fig. 61 ***Stator***

The stator:

- Remains fixed
- Contains the rotor and the winding phases

4.3.2 Rotor

The Rotor 3D model is as shown in in Fig 53.

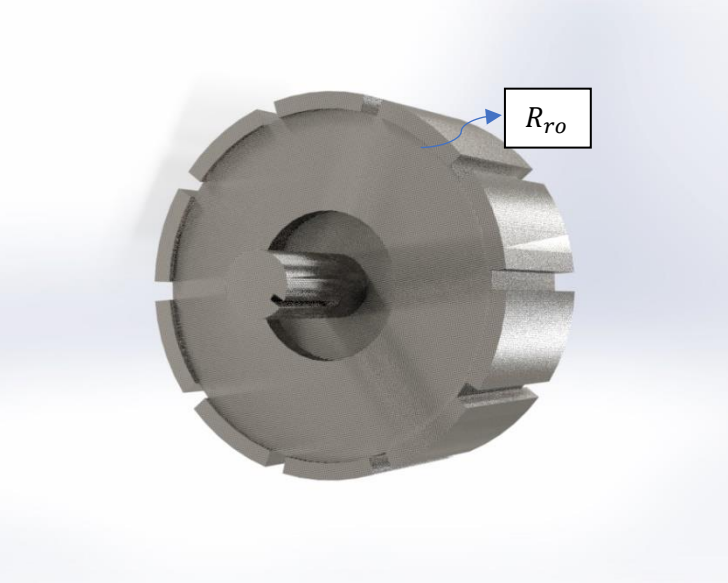

Fig. 62 ***Rotor***

The rotor:

- Rotates attached to the Cycloid drive Output Mechanism
- Has the magnets mounted over it.

4.4 Final position in the EV-TEC suspension

The final position in the suspension EV-TEC as was demonstrated in Chapter 3.3, is in position 1. The Cycloid and Electric Motor can be mounted in both corners of the suspension, but not in the front suspension because it might interfere with the direction system.

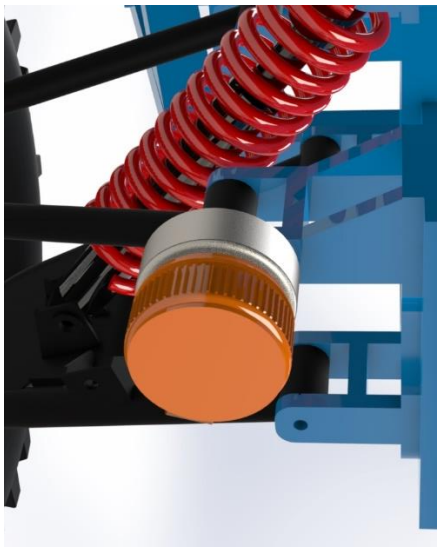

Fig. 63 ***Cycloid drive and Electric motor coupled together.***

In Fig 54 and 55 can be shown how the final model is when mounted with the two components attached together to the position 1.

Fig. 64 ***Cycloid and Electric Motor mounted in EV TEC***

- There is plenty of space enough in the Rear suspension for positioning the regenerative mechanism because the radial dimension of the Cycloid and Electric Motor is 90 mm and from position 1 to the frame there are 220 mm of distance.
- Notice that both the Cycloid and Electric motor were coupled and mounted ideally, because the main purpose of this Work was to determine the volume of both components and in which positions, they will be attached.
- It can be shown that there is no interference with other systems of the suspension.

4.5 Discussion

In this section the discussion of the results of the obtained values of the optimization for the Cycloid Drive and Electric Motor takes place.

4.5.1 Cycloid Drive and electric Motor Model

There has not been any work related to Energy harvesting using a Cycloid Drive connected to an Electric Motor. The proposed design was determined with 5 design variables and one objective function. The design variable of the diameter is the radius for the Electric Motor model, so that both components have the same radial size. Cycloid Drives are known for being great for limited space tasks in robotics, so it perfectly fits with the objective of this project. The obtained volume of 1.13e-04 m^3 is great because it doesn't cause interference with the suspension and fits perfectly

with its 89.5 mm of diameter in position 1 knowing that the distance from position 1 to the frame is 220 mm. Both components have almost the same length, but this was not planned in the design methodology. Due to fact that their diameter is greater than their length both components have a disk-shaped form which is something required for this type of tasks as stated in the state of the art.

It's important to mention that with the validation results and the values obtained in chapter 2 with the simulations. It's feasible to substitute a regular shock absorber with the cycloid regenerative shock absorber due to the slight differences between them.

5 Conclusion and Future work

This chapter aims to generalize the obtained results in this research work. The research questions and the objectives are to be answered in this chapter.

5.1 Conclusion

Based on the results obtained in the Optimization Output, it can be stated that the main and objectives have been satisfied. The solution obtained for the volume values of the Cycloid drive and the Electric Motor together fit with no problems in the suspension of the EV-TEC.

For the Cycloid Drive a value for D_z of 89.5 mm was obtained which determines the diameter of the component, and for the Electric motor. In terms of the axial length, for both together is 65.5 mm, and a total volume of 4.35e-04 m^3.With this size dimensions disk-shaped components are obtained.

The validations comparison with the theoretical give a slight difference in results and because of this, can be stated that is feasible that the Cycloid regenerative shock absorber substitutes a regular shock absorber based on the results performed in this work.

The Electric Motor design is capable of dealing with the requirements of the Skyhook necessities, showing that the analysis, methodology in this work is right.

To conclude, the Cycloid regenerative shock absorber can be used as a regular shock absorber in a suspension and regenerate energy as well. Due to its small volume can fit in probably other suspensions depending on the type of suspension and the amount of space free. Knowing that there is no other rotative regenerative damper with a Cycloid Drive this can be a revolutionary and a motivation to do more research.

The following questions were answered through the development of this work:

- **Is a Cycloid regenerative shock absorber suitable for replacing a regular shock absorber?**

During the validation, the results obtained for the road handling and weighted acceleration with the Cycloid Drive and Electric Motor for the Skyhook and Groundhook configuration were similar to the values obtained in the simulations in chapter 2, so it's feasible that the regenerative shock absorber can replace a regular shock absorber.

- **Can a cycloid regenerative shock absorber design satisfy the required constraints for a vehicle damping task?**

  The design of the Cycloid regenerative shock absorber final volume is 3.23e-04 m^3 with 89.5 mm of diameter and knowing that from the position 1 to the next body which is the frame there is 220 mm there is no possible interference, and the Cycloid Regenerative shock absorber can work normally.

5.2 Future Work

In this section, four possible topics are described to continue with the expansion of this research work.

- Implement a controller for the Electric Motor to determine the proper manage of the phases.
- Propose a validation test of the values obtained in this work with Carsim to make comparisons.
- Investigate about the manufacturing process that could be optimal for the proposed components with different materials.
- Investigate the efficiency, backlash and friction of the Cycloid Drive an Electric Motor and compare them with other gear boxes that are suitable for the tasks.

References

[1] P. T. A. RicardoFaria, "A sustainability assessment of electric vehicles as a personal mobility system". 2012.

[2] Y. a. H. H. Okada, "Regenerative Control of Active Vibration Damper and Suspension Systems. Proceedings of 35th IEEE Conference on Decision and Control". 1996.

[3] K. D. C. &. X. Yuxin Zhang, "Energy conversion mechanism and regenerative potential of vehicle suspensions". January 2017.

[4] L. X. M. K. A. A. A. E. J. M. ,. S. G. Y. L. ,. L. Z. Mohamed A.A. Abdelkareema, "Vibration energy harvesting in automotive suspension system: A detailed review". 14 April 2018.

[5] S. r. s. a. testing, "Speedgoat," 2007. [Online]. Available: https://www.speedgoat.com/success-stories/speedgoat-user-stories/clearmotion.

[6] Audi, "Audi," April 2017. [Online].

[7] P. Anne Maczulak, *Renewable Energy - Sources and Methods,* MIT, 2010.

[8] G. Morello, The Automotive Chassis, vol. II, Springer, 2019.

[9] S. M. Savaresi, Semi-Active Suspension Control Design for Vehicles, 2010.

[10] Y. X. W. P. J. Xing, "Passive–active vibration isolation systems to produce zero or infinite dynamic modulus: theoretical and conceptual design strategies," 2005.

[11] BWI, "Passive Shock Absorbers and Struts," BWI, 2019. [Online]. Available: https://www.bwigroup.com/passive-shock-absorbers-and-suspension-struts/.

[12] D. RYBA, "Semi-active Damping with an Electromagnetic Force Generator," 2007.

[13] t. Bilstein, "Advanced Semi-Active and Active Damper Technology," 2019.

[14] facomunicacion, "facomunicacion," 25 11 2014. [Online]. Available: https://www.facomunicacion.com/noticias/nuevo-volvo-xc90-equipado-con-una-suspension-inteligente-monroe.html.

[15] X. G. P. J. Y. Z. H. D. L. Y. T. X. JingyunYin, "Influence of the Li–Ge–P–S based solid electrolytes on NCA electrochemical performances in all-solid-state lithium batteries," 2015.

[16] L. Z. &. P. S. Zhang, "Energy Harvesting, Ride Comfort, and Road Handling of Regenerative Vehicle Suspensions". February 2013.

[17] B. S. J. S. a. Y. Z. Lei Zuo, "Design and characterization of an electromagnetic energy harvester for vehicle suspensions," 2010.

[18] R. O. R Gherca, "Harvesting vibration energy by electromagnetic induction," 2011.

[19] M. Meca, "Mech Meca," 2013. [Online]. Available: http://mechmecca.blogspot.com/2013/03/bose-suspension-system.html.

[20] P. G. I. a. D. T. Kynan E. Graves, "Electromagnetic regenerative damping in vehicle suspension systems," 2004.

[21] X. Wang, Frequency analysis of vibration energy harvesting systems, 2016.

[22] C. Motion, Clear Motion, 2021. [Online]. Available: https://www.clearmotion.com/.

[23] I. O. f. Standardization, Mechanical Vibration and Shock—Evaluation of Human Exposure to Whole-Body, 1997.

[24] L. Zuo, Low Order Continuous-Time Filters for proximation of the ISO 2631-1 Human Vibration Sensitivity Weightings,", 2003.

[25] R. F. Escalera, "Diseño y Construccion de un Sistema de Direccion Automatizada para un Vehiculo Eléctrico," Tec de monterrey, Monterrey, 2014.

[26] S. C. L. V. D. B. V. D. L. Elias Saerens, "Scaling laws for robotic transmissions," 2019.

[27] M. M. A. G, "Motor Catalog Program 2017/18: High Precision Drives and Systems,," 2018.

[28] D. E. G. a. P. S. Motion Technology Catalog Brushless and Brush Motors, "Moog Components Group," 2014.

[29] Neugart GmbH, "Precision gearbox catalog," 2017.

[30] F. C. Z. B. S. R. -. catalog, "Sumitomo Drive Technologies," 2011.

[31] C. &. C. S. C. S. a. H. U. -. catalog, "Harmonic Drive LLC," 2006.

[32] M. K. N. M. B. S. Z. D. L. I. V. M. M. BLAGOJEVIC, "INFLUENCE OF THE FRICTION ON THE CYCLOIDAL," Journal of the Balkan Tribological Association, Kragujevac, 2012.

[33] Q. Q. G. C. S. J. a. Y. C. Yaliang Wang, "Multi-objective optimization design of cycloid pin gear planetary reducer," 2017.

[34] L. W. a. C. S. Xi QK, "Optimized design of cycloid reducer based on genetic algorithm," *J Mech Transm ,* 2014.

[35] R. ZG, Designing of mechanism for planetary gearing, Beijing, China, 1994.

[36] D. D. Hanselman, Brushless Permanent Magnet Motor Design, 1994.

[37] D. D. Hanselman, Brushless Permanent Magnet Motor Design, 2006.

[38] prueba, prueba.

[39] M.-B. -. Domenikss, "MERCEDES-BENZ TECHNOLOGIES: MAGIC BODY CONTROL," 2016. [Online]. Available: https://www.domenikss.lv/en/about-us/news/mercedes-benz-technologies-magic-body-control-31.

[40] Toyota, "Toyota Mexico," 2022. [Online]. Available: https://toyota.mx/modelo/corolla?gclid=Cj0KCQiArt6PBhCoARIsAMF5waguqq1fJ5cS12JXjlHLorsTYO_N-tqrrao0djsOtvXCLH-pMNAD_7saAhE4EALw_wcB.

[41] F. &. H. Y.-F. &. T. S.-H. &. J. W. Tyan, "隨機路面之產生 Generation of Random Road Profiles. Journal of Advanced Engineering.," 2009.

[42] Y. K. L. V. S. G. Rakshith M, "Bose Automotive Suspension," *International Journal of Recent Technology and Engineering (IJRTE),* 2014.

[43] B. S. J. S. a. Y. Z. Lei Zuo, "Design and characterization of an electromagnetic energy harvester for vehicle suspensions," 2010.

[44] P. G. I. a. D. T. Kynan E. Graves, "Electromagnetic regenerative damping in vehicle suspension systems," 2004.

[45] F. N. A. A. M. F. Huber J. E., "The selection of mechanical actuators based on performance indices".

[46] J. H. J. B. I.W. Hunter, "A comparative analysis of actuator technologies for robotics, Robot.," 1991.

[47] S. X. A.J. Veale, " Towards compliant and wearable robotic orthoses: areview of current and emerging actuator technologies," 2016.